



ChemComm

**A fresh perspective on metal ammonia molecular complexes  
and expanded metals: Opportunities in catalysis and  
quantum information**

Journal:	<i>ChemComm</i>
Manuscript ID	CC-FEA-06-2023-002956.R1
Article Type:	Feature Article

SCHOLARONE™  
Manuscripts

## ARTICLE

# A fresh perspective on metal ammonia molecular complexes and expanded metals: Opportunities in catalysis and quantum information

dReceived 00th January 20xx,  
Accepted 00th January 20xx

DOI: 10.1039/x0xx00000x

Benjamin A. Jackson,<sup>a</sup> Shahriar N. Khan,<sup>a</sup> and Evangelos Miliordos<sup>\*a</sup>

Recent advances in our comprehension of the electronic structure of metal ammonia complexes have opened avenues for novel materials with diffuse electrons. These complexes in their ground state can host peripheral “Rydberg” electrons which populate a hydrogenic-type shell model imitating atoms. Aggregates of such complexes form the so-called expanded or liquid metals. Expanded metals composed of *d*- and *f*-block metal ammonia complexes offer properties, such as magnetic moments and larger numbers of diffuse electrons, not present for alkali and alkaline earth (*s*-block) metals. In addition, tethering metal ammonia complexes via hydrocarbon chains (replacement of ammonia ligands with diamines) yields materials that can be used for redox catalysis and quantum computing, sensing, and optics. This perspective summarizes the recent findings for gas-phase isolated metal ammonia complexes and projects the obtained knowledge to the condensed phase regime. Possible applications for the newly introduced expanded metals and linked solvated electrons precursors are discussed and future directions are proposed.

## 1. Introduction

Electrons are the currency used in the molecular world. They are exchanged or shared during atomic or molecular interactions (chemical bonding),<sup>1</sup> or they can be deposited as anions in solvent banks (solvated electrons).<sup>2</sup> Depending on the morphology of the potential energy well they reside at, bound electrons may be highly localized or dispersed extensively in space. Intermediate to these two is the case of delocalized electrons in aromatic systems (Hückel, Möbius,<sup>3</sup> or Hirsh<sup>4</sup>) or polarized electrons in intermolecular interactions.<sup>3</sup>

Diffuse electrons can also be found in materials, such as electrides (organic or inorganic) and expanded (or liquid) metals.<sup>5,6</sup> The categorization of these materials is based on the different molecular skeletons. The building units of organic electrides are (usually alkali) metal coordination complexes with organic molecules as ligands, which are surrounded by electrons trapped in the formed cavities or pores. Typical organic ligands are crown ethers<sup>7-9</sup> or cryptands<sup>6,10</sup> while azacrown ethers have recently been investigated theoretically.<sup>11,12</sup> Inorganic electrides are usually one,<sup>13</sup> two, or three dimensional crystals with electrons in void spaces or two-dimensional crystalline sheets separated by a layer of diffuse electrons. These are commonly composed of alkali, alkaline earth, aluminum, oxygen and nitrogen atoms,<sup>6</sup> or even metallic clusters.<sup>14</sup> Expanded metals are similar to organic electrides<sup>15</sup> but the ligands are solvent molecules known to solvate electrons, such as ammonia,<sup>5</sup> water,<sup>16-20</sup> dimethyl ether,<sup>21,22</sup>

methanol,<sup>23,24</sup> methylamine,<sup>25-31</sup> acetonitrile,<sup>32</sup> hexamethylphosphoric triamide (HMPA)<sup>33,34</sup> and tetra-hydrofuran.<sup>35</sup> Electrides and expanded metals can be unified under the general category of solvent separated electrons from metals ions.<sup>15</sup>

Among these species, electrides have been studied quite extensively both experimentally and computationally.<sup>36</sup> Crystal structures are reported for multiple systems and various applications have been proposed in the literature.<sup>37-42</sup> On the other hand, our knowledge for the expanded metals is less extensive.<sup>5</sup> Expanded metals have been observed for a handful of systems Li/(NH<sub>3</sub>,CH<sub>3</sub>NH<sub>2</sub>), (Na,K,Cs,Ca,Sr,Ba,Eu,Yb)/NH<sub>3</sub>.<sup>43-45</sup> The crystal structure is known in detail only for lithium,<sup>29,46</sup> and only recently possible applications have been suggested based on *in silico* results.<sup>47,48</sup> The present article focuses on metal-ammonia expanded metals aspiring to serve as motivation for future work on these materials based on recent *ab initio* results and demonstrating possible advantages over electrides. More detailed reviews on electrides can be found in refs <sup>6,37</sup>.

We will continue (Section 2) with a detailed account on the electronic structure, stability, and computational challenges for the building blocks (focusing on isolated metal ammonia complexes or so-called solvated electron precursors = SEPs) of expanded metals. This discussion extends to the various regions of the periodic table (*s*-, *p*-, *d*-, and *f*-blocks) going beyond the usually reported alkali and alkaline earth metals. Section 3 discusses the formation of crystalline materials from SEPs, and section 4 refers to possible applications including catalysis, electronic devices, and quantum information systems. Section 5 summarizes the main points and provides a personal outlook to future directions. Although this account is based on results reported already in the literature, some calculations have been

<sup>a</sup> Department of Chemistry and Biochemistry, Auburn University, Auburn, AL 36849-5312, USA. E-mail: [emiliord@auburn.edu](mailto:emiliord@auburn.edu)

done presently with Gaussian16<sup>49</sup> (unless otherwise noted). The discussion that follows impacts various fields, such as molecular physics, electronic structure theory, materials, chemistry in solutions, gas-phase experiments, and chemical education.

## 2. The Molecular Building Units

**Electronic structure model.** The simplest metal ammonia complex bearing a diffuse electron is  $\text{Li}(\text{NH}_3)_4$  wherein a single electron occupies a diffuse orbital which surrounds the periphery of the complex (see orbital 1s in Figure 1). Such a system is an example of the solvated electron precursor or SEP. Sommerfeld and Dreux who examined the density of the diffuse s-type orbital (see orbitals 1s in Figure 1) showed that only 2% of this density is within the covalent radius of lithium (1.82 Å).<sup>50</sup> The same value for the lithium atom is 45%, for  $\text{Li}(\text{NH}_3)$  is ~33%, for  $\text{Li}(\text{NH}_3)_2$  ~10%, for  $\text{Li}(\text{NH}_3)_3$  ~5% and indicating a gradual depletion of the lithium valence space of electronic density. The penetration of the diffuse electron into each ammonia ligand is even smaller (~1%) in absolute agreement with the findings in anionic pure ammonia clusters.<sup>51</sup>

The same observation was made for the  $\text{Ca}(\text{NH}_3)_{0.8^+}$  species looking at the contours of the outer diffuse orbital.<sup>52</sup> The corresponding radial distribution plots for the neutral calcium ammonia complexes (along a path which avoids the ammonia ligands) revealed a gradually higher diffusion of the density to longer distances for up to five ammonia ligands. For six and more ammonia ligands there is a sudden shift of the maximum of these plots from about 2 Å to 4 Å signaling the displacement of the electron from the valence space of calcium to the periphery of the complex.<sup>52</sup> Similar plots for V and  $\text{V}(\text{NH}_3)_6$  demonstrated that the valence 4s orbital “swells” by 2 Å due to the presence of the ammonia ligands.<sup>52</sup>

Three models exist for explaining the origin of this diffuse orbital: the metal-centric, the ligand-centric, and the expanded atom.

The metal-centric model attributes the diffuse orbital as a metallic orbital, which is perturbed by the ligand field. This model is supported by the radial distribution plots for the electronic density  $P(r)$  of the outer electron. For example, Zurek et al. also indicates that “The likeliest place to find the electron in  $\text{Li}(\text{NH}_3)_4$  lies almost midway between the maximum  $P(r)$  for an electron in the Li (gas-phase) atomic 2s and 3s orbitals”.<sup>5</sup> The exact same conclusion can be inferred from the plots of Figure 3 in ref. <sup>52</sup> regarding  $\text{V}(\text{NH}_3)_6$ , where the diffuse electron is more likely to be found midway between the valence (4s) and next s-type (5s) orbitals.

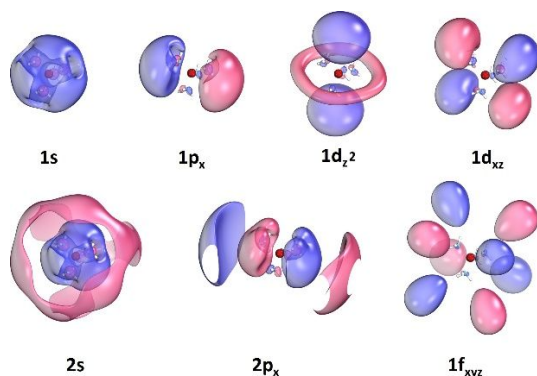


Figure 1. Low-lying peripheral “Rydberg” orbitals of  $\text{Li}(\text{NH}_3)_4$ .

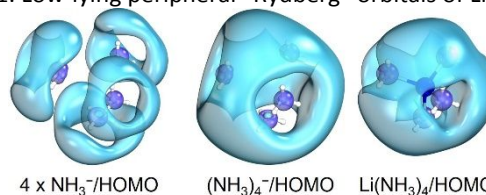


Figure 2. HOMO orbitals for  $\text{NH}_3^-$ ,  $(\text{NH}_3)_4^-$ , and  $\text{Li}(\text{NH}_3)_4$ .

The ligand-centric model has been suggested by Zurek, Edwards, and Hoffmann,<sup>5</sup> viewing  $\text{Li}(\text{NH}_3)_4$  as  $\text{Li}^+(\text{NH}_3)_4^-$ . According to this picture the electron belongs to the ammonia cluster bearing this specific tetrahedral geometry. Ammonia clusters are known to solvate electrons albeit with minimal electron affinities. For example, the global minimum (“linear” arrangement) of  $(\text{NH}_3)_4^-$  has a vertical detachment energy of ~60 meV (calculated with CCSD(T)).<sup>51</sup> In the case of  $\text{Li}(\text{NH}_3)_4$ , the  $\text{Li}^+$  center stabilizes the tetrahedral  $(\text{NH}_3)_4^-$  system. In addition, Zurek *et al.* calculated the radial distribution of the probability  $P(r)$  for the diffuse electron in Li ( $2s^1$  and  $3s^1$  states),  $\text{Li}(\text{NH}_3)_4$ , and  $(\text{NH}_3)_4^-$ . They found that the degree of diffusion follows the order  $\text{Li}(2s^1) < \text{Li}(\text{NH}_3)_4 < \text{Li}(3s^1) < (\text{NH}_3)_4^-$  indicating that the  $(\text{NH}_3)_4^-$  orbital is substantially contracted due to the presence of  $\text{Li}^+$ . Figure 2 shows the HOMO orbitals of four  $\text{NH}_3^-$  ions in the geometry of  $(\text{NH}_3)_4^-$ , which can be “combined” to produce the HOMO of  $(\text{NH}_3)_4^-$ , which contracts in the presence of  $\text{Li}^+$  to the HOMO of  $\text{Li}(\text{NH}_3)_4$ .

The authors and collaborators argue that a “fairer” interpretation is the expanded atom model which attributes the electron as belonging to the whole of the molecular complex. This is first demonstrated in ref. <sup>53</sup> where the isoivalent  $\text{Be}(\text{NH}_3)_4^+$  is studied alongside a hypothetical model of one electron exposed to the electrostatic potential produced by  $\text{Be}^{2+}(\text{NH}_3)_4$ . The numerical solution of the Schrödinger equation was able to reproduce the electronic structure of the system for its ground and excited electronic states (see below). This viewpoint perceives SEPs as “expanded atomic” entities where the metal-ammonia skeleton acts as an “expanded nucleus” of the system suggesting that SEPs can form “expanded molecules” by binding together through “expanded covalent” bonds (see below). Similar concepts have been expressed for the so-called superatoms, which are metallic clusters with electronic structure resembling that of hydrogen.<sup>54, 55</sup>

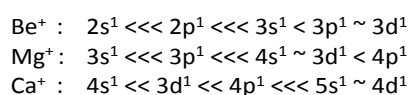
The concept of the “expanded atom” is supported by the excited states of these systems. The lowest energy outer s-type orbital has been dubbed 1s, which is followed by the 1p, 1d, 2s, 2p, and 1f orbitals (see Figure 1). The pattern is nearly identical for all metal-ammonia and metal-water species studied so far,<sup>52, 53, 56-58</sup> indicating that the metal identity is suppressed and that the outer electrons experience the metal more as a central charge. Note that the numbers do not correspond to a quantum number but to the cardinality within each orbital type. Similarly, the s, p, d, f symbols refer to the shape and near-degeneracy of the orbitals and not strictly to the angular momentum, which in principle is not conserved in these systems. However, the calculated transition electric dipole moments follow the well-known selection rules of atomic spectroscopy. For example, the  $1s \rightarrow 1p$  transitions are very strong, unlike  $1s \rightarrow 1d$ .<sup>58, 59</sup>

The degeneracy among the 1d orbitals is not exact. The tetrahedral or pseudo-octahedral symmetry elements in  $\text{Li}(\text{NH}_3)_4$  or  $\text{Ca}(\text{NH}_3)_6$ , respectively, allow only up to triple

degeneracy. Thus, the 1d orbitals split into the ( $d_{xy}$ ,  $d_{xz}$ ,  $d_{yz}$ ) and ( $d_{x^2-y^2}$ ,  $d_{z^2}$ ) groups, which differ energetically by just 0.01 eV.<sup>52, 58</sup> The same splitting for  $V(NH_3)_6^+$  is 0.1 eV,<sup>52</sup> and for the low-symmetry  $Ca(H_2O)_6$  complex is 0.4 eV.<sup>60</sup> The splitting in the 2d states of the latter drops to 0.05 eV<sup>60</sup> because of the larger size of 2d. The 2d<sup>1</sup> electrons are further from the metal center and the structural features of the  $Ca(H_2O)_6^{2+}$  core are less “visible” by the 2d<sup>1</sup> electrons.

The calculated Aufbau principle for SEPs matches closely the Jellium shell model used to explain the electronic structure of electrons delocalized in metallic clusters (superatoms).<sup>61, 62</sup> It also resembles the nuclear shell model used to provide the levels populated by protons and neutrons in atomic nuclei.<sup>63</sup> The notation used and the energy order found for SEPs, superatoms, and nuclei are identical, and seem to indicate that the observed common shell model is very general, and not system specific. On the other hand, the hydrogenic model (1s, 2s, 2p, 3s, 3p, 3d, etc.) is valid only for central Coulombic potential. Comparing the two cases, we see that the Coulomb potential destabilizes higher angular momentum orbitals. For example, f-type orbitals appear in the fifth electronic state of SEPs (1f) but appear much higher for hydrogenic species (4f).

This SEP-shell model remains consistent for the various metal ammonia complexes studied so far,<sup>52, 53, 56, 58, 64-66</sup> despite the differing electronic structure of the metals. Specifically, the lowest energy states of the lighter alkaline earth metal cations are:



where  $\lll$  /  $\ll$  /  $<$  denote energy differences of more than 20,000  $cm^{-1}$  / 10,000  $cm^{-1}$  / 5,000  $cm^{-1}$ , respectively, and the “ $\sim$ ” means less than 5,000  $cm^{-1}$ .<sup>67</sup> Upon saturation with the ammonia ligands (complete first solvation shell) the orbitals’ order switches to  $1s^1 < 1p^1 < 1d^1 < 2s^1 \sim 1f^1 \sim 2p^1$  for all species.<sup>52, 53</sup>

To illustrate the effect of ligand coordination in the metal ammonia complexes, we constructed the potential energy profiles (PEPs) for the concerted approach of four ammonia ligands to  $Be^+$ ,  $Mg^+$ , and  $Ca^+$  in a tetrahedral arrangement to form  $Be(NH_3)_4^+$ ,  $Mg(NH_3)_4^+$ , and  $Ca(NH_3)_4^+$ . The PEPs for the lower energy states of the tetra-coordinated complexes are shown in Figure 3. An immediate observation is that the two PEPs pertaining to  $ns^1$  and  $(n+1)s^1$  ( $n = 2, 3, 4$  for  $Be^+$ ,  $Mg^+$ ,  $Ca^+$ ) undergo some avoided crossing at a metal-nitrogen distance 0.5 Å longer than the equilibrium bond length. The avoided crossing is a result of the  $ns$  valence orbital mixing with the  $(n+1)s$  or higher s-type metallic orbitals to form the outer 1s orbital of the complex. This agrees with earlier discussion on the radial distribution of the outer 1s orbital for  $Li(NH_3)_4$  and  $V(NH_3)_6$ . Here, the effect is most evident for  $Be^+$  and nearly vanishes for  $Ca^+$ .

On the other hand, the  $1p^1$  or  $1d^1$  states of the complexes transition from the  $np^1$  and  $3d^1$  or  $4d^1$  metallic states in a smooth manner. The exact same trends were seen for the  $Sc(NH_3)_6^{2+}$  complex.<sup>66</sup> The connection between  $1p^1/1d^1$  states of  $Ca(NH_3)_4^+$  and  $3d^1/4p^1$  states of  $Ca^+$  is a special case. The  $3d^1$  states are lower than  $4p^1$  but the corresponding  $1d^1$  states are higher than  $1p^1$ . Therefore, the  $4p^1$  and the three same-symmetry  $3d^1$  states ( $t_2$  orbitals in  $T_d$  point group) blend

together in the 2.6–4.0 Å region, and the two PEPs (blue and red in Figure 3) exchange characters at equilibrium. The two  $3d^1/e$  components transition smoothly to the  $1d^1/e$  ones, and at equilibrium the e and  $t_2$  components of  $1d^1$  state become nearly degenerate and higher in energy than  $1p^1$ .

Based on these observations, we consider that the picture of “expanded atoms” is more representative, and that the addition of ammonia ligands modifies the electronic structure of the system dramatically. Additional support for this picture is given by the considerable changes in the excitation energies and binding energies when the first solvation shell is saturated. Specifically, going from  $Ca(NH_3)_5^+$  to  $Ca(NH_3)_6^+$ , the excitation energy for the first excited state is halved, indicating that the electron has significant metallic character in the former case, which diminishes in the second case.<sup>52</sup> The excitation energy

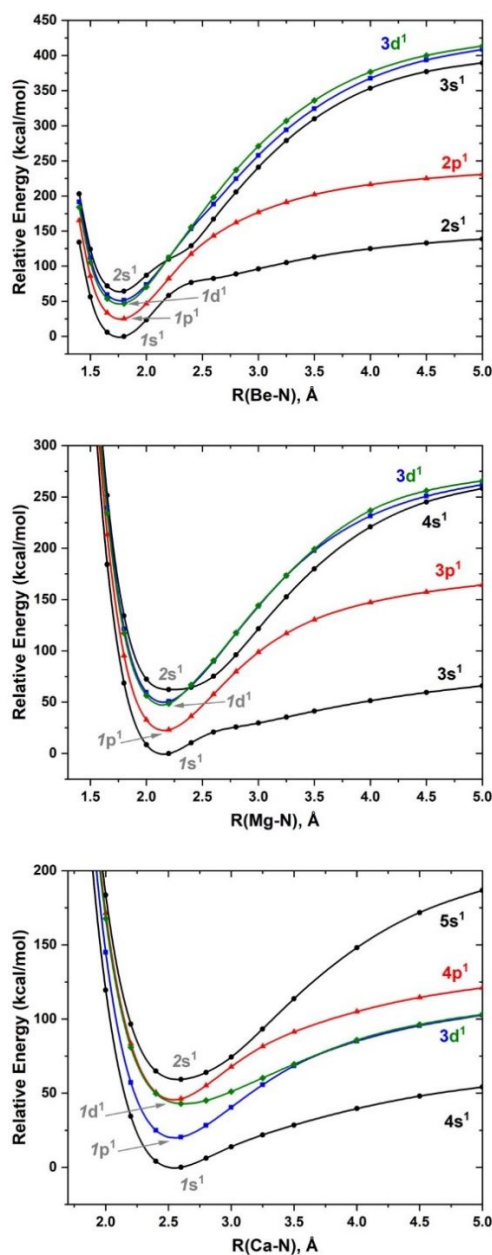


Figure 3. CASSCF potential energy profiles for the concerted

attachment of four ammonia ligands (tetrahedral arrangement) to  $\text{Be}^+$ ,  $\text{Mg}^+$ , and  $\text{Ca}^+$  in various electronic states.

remains unaffected going to  $\text{Ca}(\text{NH}_3)_7^+$  and  $\text{Ca}(\text{NH}_3)_8^+$ . The radial distribution function of the electronic density reveal also that the outer electron is suddenly jostled away from the metal going from  $\text{Ca}(\text{NH}_3)_5^+$  to  $\text{Ca}(\text{NH}_3)_6^+$  (see Figure 2 of ref. <sup>52</sup>). Further, we see the N-H stretching frequency of the ammonia ligands decreases with increasing coordination until the sixth ammonia where frequency then increases (see Figure 3 of ref. <sup>52</sup>). Finally, the detachment energy of an ammonia ligand is larger (almost double) for  $\text{Ca}(\text{NH}_3)_6$  compared to  $\text{Ca}(\text{NH}_3)_5$  (see Table 1 of ref. <sup>52</sup>).

While the full saturation of the first coordination sphere occurs at four, six, and eight ammonia ligands for beryllium, magnesium, and calcium, the transition to an expanded metal may occur at lower coordination numbers. For example, magnesium's transition occurs at four-coordination and calcium at six-coordination.<sup>52, 53, 68</sup> For consistency, the PEPs of Figure 3 correspond to the tetrahedral tetra-coordinated species for all metals for consistency. The tetrahedral  $\text{Ca}(\text{NH}_3)_4^+$  species also has a peripheral 1s electron but it is not a real minimum in the potential energy surface, which prefers the planar conformation by 5.2 kcal/mol (present calculations at B3LYP/aug-cc-pVDZ).  $\text{Mg}(\text{NH}_3)_4^+$  is an actual minimum and has one 1s electron, but it is 1.6 kcal/mol higher than the global minimum  $\text{Mg}(\text{NH}_3)_3(\text{NH}_3)_1^+$ , i.e. one ammonia is placed in the second solvation shell and the electron is on the metal.<sup>69</sup>

Based on the PEPs of Figure 3, the displacement of the more diffuse valence s-electron of  $\text{Ca}^+$  (compared to  $\text{Be}^+$  and  $\text{Mg}^+$ ) is smoother but leads to smaller metal-ammonia binding energies due to the smaller charge density of the  $\text{Ca}^{2+}$  core. Specifically, the binding energy per metal-ammonia bond is 47.0, 26.9, and 21.0 kcal/mol for  $\text{Be}^+$ ,  $\text{Mg}^+$ , and  $\text{Ca}^+$ , respectively, at CCSD(T)/aug-cc-pVTZ//B3LYP/aug-cc-pVDZ level of theory. The same values for Li and Na are 14.2 and 7.9 kcal/mol. If we plot the binding energies as a function of the charge density ( $+2/r_{\text{ion}}^3$ ,  $r_{\text{ion}}$  = ionic radius) for the three alkali metal dications (ionic radii taken from ref. <sup>70</sup>; 0.59, 0.86, and 1.14 Å for  $\text{Be}^{2+}$ ,  $\text{Mg}^{2+}$ , and  $\text{Ca}^{2+}$ , respectively) we see a linear relation between the two ( $r^2=0.9999$ ).

The attack of four ammonia molecules against a “two-electron” species, such as neutral Be atom, is not barrier-free. The simultaneous approach in  $\text{Be}(\text{NH}_3)_4$  has to overcome a barrier of 18.2 kcal/mol, after which there is a well of 75 kcal/mol (see Figure 2 of ref. <sup>53</sup>). Interestingly, if the formation

$[\text{Li}(\text{NH}_3)_4(\text{NH}_3)_{12}]$  solvation shells.<sup>58, 65</sup> The 1f states for  $\text{Li}(\text{NH}_3)_4$  were not identified by the authors of ref. <sup>58</sup>.

of  $\text{Be}(\text{NH}_3)_4$  occurs in two steps [ $\text{Be} + 3\text{NH}_3 \rightarrow \text{Be}(\text{NH}_3)_3$  and  $\text{Be}(\text{NH}_3)_3 + \text{NH}_3 \rightarrow \text{Be}(\text{NH}_3)_4$ ] the two barriers are smaller, 13 kcal/mol (see Figure 5 or ref. <sup>71</sup>) and less than 2 kcal/mol (see Figure 2 of ref. <sup>53</sup>), meaning that after the insertion of three ammonia ligands, the 2s electrons are quite diffuse facilitating the insertion of the fourth ligand.

A similar story is shown in the  $\text{V} + 6\text{NH}_3$  PEPs (see Figure 5 of ref. <sup>52</sup>). The ground state of V is a  $^4\text{F}$  with a  $4s^23d^3$  configuration and its first excited state is a  $^6\text{D}$  of  $4s^13d^4$  configuration. The barrier to displace the two 4s electrons of the  $^4\text{F}$  is comparable to  $\text{Be}(\text{NH}_3)_4$  ( $\sim 20$  kcal/mol)<sup>52</sup> but to displace the one 4s electron of  $^6\text{D}$  is nearly half that (8 kcal/mol)<sup>52</sup>. However, the potential energy well of the  $^4\text{F}$  is nearly twice that of  $^6\text{D}$  ( $\sim 60$  vs  $\sim 30$  kcal/mol)<sup>52</sup> owing to the greater metal charge [ $\text{V}^{2+}(3d^3)$  for  $^4\text{F}$  vs.  $\text{V}^+(3d^4)$  for  $^6\text{D}$ ].

Looking at the metal ammonia complexes from a distance we can see the diffuse electrons in a spherical globe with a positively charged center. Therefore adding a second solvation shell to  $\text{Li}(\text{NH}_3)_4$ , for example, this sphere becomes larger (the radius of the molecular skeleton approximately doubles, Li to terminal H atoms distance is  $r \approx 6.5$  Å vs.  $r \approx 3.0$  Å)<sup>65</sup> and at the same time the effective central/metallic charge ( $Z$ ) drops due to the electrostatic screening of the intervening ammonia ligands. Based on the virial theorem for the hydrogenic atoms ( $E_n = -\langle V \rangle = -1/2 Ze^2 \langle 1/r \rangle_n$ ), the excitation energies are expected to become half or less. Indeed, the energy diagram of Figure 4, which compares the excitation energies of  $\text{Li}(\text{NH}_3)_4$  and  $\text{Li}(\text{NH}_3)_4(\text{NH}_3)_{12}$ , reveals a decrease by a factor of  $2.4 \pm 0.4$ . In both cases the  $1s \rightarrow 1p$  excitation happens in the infrared region as opposed to the solvated electron in low concentration alkali metal ammonia solutions, which absorbs in the visible region giving the observed blue color.<sup>72</sup>

Although the literature is dominated by alkali and alkaline earth metal ammonia complexes, transition metal complexes are more fascinating and didactic. It is shown that the valence 4s or 5s electrons of first- or second-row transition metals is displaced to the periphery of the metal-ammonia molecular skeleton (see Figure 4 of ref. <sup>52</sup> and Figure 5). The implications of this observation described below are of both educational and practical importance.

General or inorganic chemistry textbooks refer to the ligand effects on the energies of the valence  $d$ -orbitals and how this modifies the electronic structure and chemical reactivity of these species. The fate of the valence  $s$ -orbital when ammonia ligands bind to the metal center is generally overlooked. Ammonia is considered a strong-field ligand inducing a large

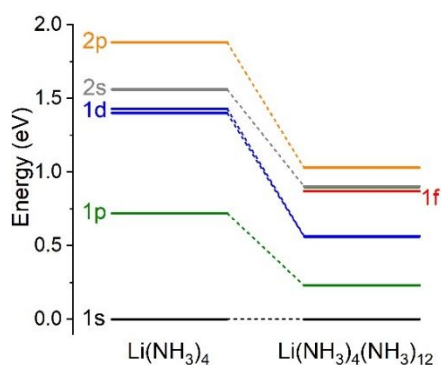


Figure 4. Energy levels for the lowest electronic states of lithium-ammonia complexes with one  $[\text{Li}(\text{NH}_3)_4]$  and two

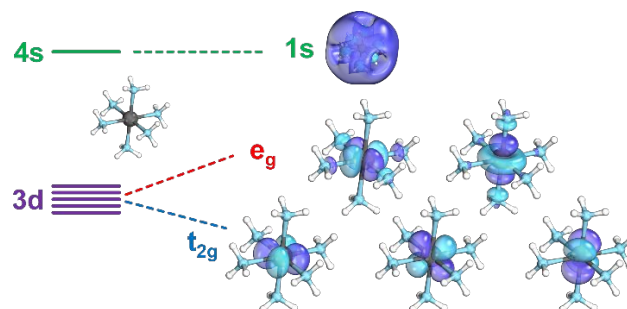


Figure 5. Transformation of the valence  $3d$  and  $4s$  orbitals of  $M(\text{NH}_3)_6$ , where  $M$  is a first-row transition metal atom. The  $1s$  outer orbital is populated before the  $e_g$  orbitals.

splitting among the  $d$ -orbitals. At the same time, the valence  $s$ -orbital becomes the outer- $1s$  orbital, which can be populated before higher energy inner  $d$ -orbitals. For example, the ground state of  $\text{V}(\text{NH}_3)_6^{2+}$  has a  $3d/t_{2g}^3$  configuration, and the addition of one electron to make  $\text{V}(\text{NH}_3)_6^+$  leads to (atomic/molecular orbital notation)  $3d/t_{2g}^3 4s/1s^1$ ,<sup>52</sup> instead of  $3d/t_{2g}^4$  or  $3d/t_{2g}^3 3d/e_g^1$ . Similarly, adding one electron to  $\text{Sc}(\text{NH}_3)_6^{2+}$  ( $t_{2g}^1$ ) leads to  $\text{Sc}(\text{NH}_3)_6^+$  with  $t_{2g}^1 1s^1$  or  $1s^2$  configurations; the two states being nearly degenerate.<sup>66</sup> It should be noted that the diffuse electron in  $\text{V}(\text{NH}_3)_6^+$  can be easily captured by other species in a solution and thus its observation may require delicate experiments.

From the more practical viewpoint, transition metal-ammonia complexes are shown to have two co-existing electronic shells: The inner  $d$ -shell and the outer hydrogenic-type shell, which is identical to that observed in  $s$ -block metals ( $1s$ ,  $1p$ ,  $1d$ ,  $2s$ ,  $2p$ ,  $1f$ , etc). Electronic excitations in the outer shell happen at lower energies, and it turns out that they are independent of the electronic structure of the inner  $d$ -electrons. Specifically, quantum calculations show that the first excitation for  $M(\text{NH}_3)_6^+$  ( $M = \text{Sc}, \text{V}, \text{Cr}, \text{Mo}$ )<sup>52, 59, 66</sup> pertains to outer  $1s \rightarrow 1p$  excitations consistently at  $\sim 1.0$  eV independently of the central metal. In addition, the  $t_{2g}^3 e_g^1 1s^1 \rightarrow t_{2g}^3 e_g^1 1p^1$  and  $t_{2g}^4 1s^1 \rightarrow t_{2g}^4 1p^1$  transitions in  $\text{Mo}(\text{NH}_3)_6$  or the  $t_{2g}^3 e_g^1 1s^1 \rightarrow t_{2g}^3 e_g^1 1p^1$  and  $t_{2g}^3 e_g^1 1s^1 \rightarrow t_{2g}^3 e_g^1 1p^1$  [ $e_g = d_{z^2}$  and  $e_g' = d_{x^2-y^2}$ ] in  $\text{Cr}(\text{NH}_3)_6$  occur also at  $\sim 1.0$  eV.<sup>59</sup> The same seems to be true for the inner excitations. The  $t_{2g} \rightarrow e_g$  excitation in  $\text{V}(\text{NH}_3)_6^+$  and  $\text{V}(\text{NH}_3)_6$  occurs at  $\sim 1.7$  eV despite the fact that the former has one outer  $1s$  electron and the former has two.<sup>52</sup> The same excitation occurs at 1.4 eV in  $\text{Mo}(\text{NH}_3)_6^+$  for both  $1s^1$  and  $1p^1$  outer electronic configurations.<sup>59</sup> Conclusively, transition metal ammonia complexes retain two electronic shells, which act nearly independently.

Based on the previous observations, dissolving transition metal atoms in ammonia will create expanded metals with well protected inner  $d$ -electrons. If these electrons are unpaired, then the expanded metal will have magnetic properties unlike the alkali or alkaline earth expanded metals. More implications for future materials are given in Section 4.

Even though there is clear separation between the valence space of the metal from the outer electrons, i.e., the peripheral electrons obey to a "universal" shell model defying the character of the central metal, the nature of the metal plays an important role in the stability, composition, and electronic structure of SEPs. For example, scandium prefers hexa-coordinated ammonia complexes with two peripheral electrons, while its second-row transition metal counterpart (yttrium) prefers octa-coordinated complexes with three peripheral electrons.<sup>56, 66</sup> Hexa-coordinated chromium complexes prefer high-spin states, while molybdenum prefers low-spin states.<sup>59</sup> As we explore more systems, more of these features will be revealed, and thus the study of all metals is important.

The overall charge of the complexes is also a determining parameter. It seems that the presence of more peripheral electrons stabilizes the structures with complete first solvation shell. For instance,  $\text{Cr}(\text{NH}_3)_4(\text{NH}_3)_2^+$  is clearly lower (by about  $\sim 25$  kcal/mol) than  $\text{Cr}(\text{NH}_3)_6^+$  (one peripheral electron), but the difference drops to less than 5 kcal/mol for the neutral systems

(two outer electrons).<sup>59</sup> The binding energies are larger for the first ammonia ligands of the cationic complexes, but become comparable with those of the neutral as we approach the completion of the first solvation shell (see for example Figure 3 of ref. <sup>59</sup> for Cr/Mo and Table I of ref. <sup>52</sup> for Ca).

Although this work is focused on metal ammonia complexes due to their superior stability and existence of experimental structures and spectra, other ligands that can dissolve electrons can in principle form SEPs. As discussed later, metal-water complexes are more prone to  $\text{H}_2$  release, and water ligands prefer to populate the second solvation shell before saturating the first solvation shell (see for example the case of Mg; refs. <sup>57, 73</sup> and references therein). Other experimentally studied systems are metal-crown ether complexes (forming electriles in the condensed phase). The smaller metal-ligand binding energies and the weaker ability of ethers to solvate electrons<sup>64</sup> can lead to the formation of  $\text{Na}^-$  (alkalides) and  $\text{Na}^+$  complexes instead of SEPs (no diffuse electrons).<sup>74, 75</sup> The replacement of oxygen with nitrogen (crown ethers  $\rightarrow$  aza-crown ethers or cyclams) or polydentate nitrogen-anchored ligands (such as cryptands) should be a better choice.<sup>11, 64</sup> Less conventional suggestions are a dodecahedrane metal complex<sup>76</sup> or the "inverted" SEPs  $\text{XM}_4$  ( $X = \text{N}, \text{P}$  and  $M = \text{Li}, \text{Na}$ ).<sup>76</sup> Finally, species containing no metal atoms have been studied in the literature as well.<sup>77-80</sup>

**Stability aspects.** The previous discussion leads to the question: What are the important factors for the stability of these metal ammonia complexes with diffuse peripheral electrons? To examine this we can envision the mechanism of formation as a series of steps: First, the metal atom must be ionized to remove the diffuse-to-be electrons. Then a number of ammonia ligands coordinate to the positively charged metal core, and finally the removed electrons return to the periphery of the complex. The direct and indirect formation of SEPs is shown pictorially for  $\text{Li}(\text{NH}_3)_4$  in Figure 6. From this mechanism we can identify these stability factors as: the metal ionization energy, the strength and number of metal ligand bonds, and the ability of the ligands to solvate electrons.

As shown earlier, the binding energy decreases for metal ammonia complexes as we go from beryllium to calcium due to the stronger electrostatic attraction for the smaller  $\text{Be}^{2+}$ . Scanning over different ligands  $L$  now, the binding energies per ligand molecule for  $L = \text{NH}_3, \text{MeNH}_2, \text{H}_2\text{O}, \text{MeOH}$ , and  $\text{Me}_2\text{O}$  ( $\text{Me} = \text{CH}_3$ ) to  $\text{Be}^{2+}, \text{Be}^+$ , and  $\text{Be}$  are listed in Table 1. The binding energy to  $\text{Be}^{2+}, \text{D}_e^{(2+)}$ , is higher for ligands anchoring with

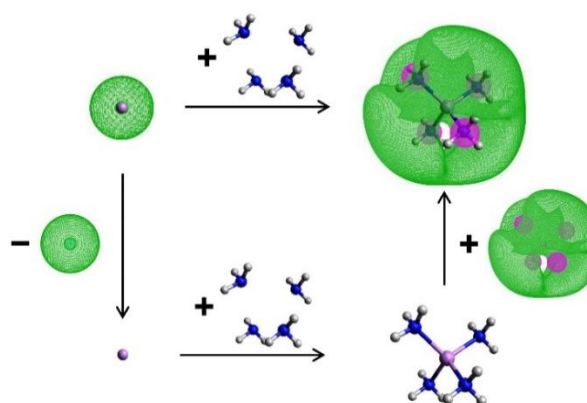


Figure 6. Formation of  $\text{Li}(\text{NH}_3)_4$  via two routes: Directly from  $\text{Li} + 4\text{NH}_3$  (top arrow), and indirectly by removing the 2s electron of  $\text{Li}$  to make  $\text{Li}^+$  (left arrow),  $\text{Li}^+ + 4\text{NH}_3$  (bottom arrow), and finally adding the outer 1s diffuse electron to the produced  $\text{Li}(\text{NH}_3)_4^+$ .

Table 1. Calculated<sup>a</sup> binding energies  $D_e$  (in kcal/mol) per metal-ligand bond and ionization energies  $IE$  (in eV) for selected  $\text{BeX}_4$  species ( $X = \text{NH}_3, \text{MeNH}_2, \text{H}_2\text{O}, \text{MeOH}, \text{Me}_2\text{O}, \text{Me} = \text{CH}_3$ ).  $D_e^{(2+)}$ ,  $D_e^{(+)}$ , and  $D_e^{(0)}$  refer to the binding energies for  $\text{Be}^{2+} + 4X \rightarrow \text{BeX}_4^{2+}$ ,  $\text{Be}^+ + 4X \rightarrow \text{BeX}_4^+$ , and  $\text{Be} + 4X \rightarrow \text{BeX}_4$ , respectively.  $IE_1$  and  $IE_2$  correspond to the first and second ionization energies of  $\text{BeX}_4$ .

X	$D_e^{(2+)}$	$D_e^{(+)}$	$D_e^{(0)}$	$IE_1$	$IE_2$
$\text{NH}_3$	111.8	47.3	16.8	3.81	7.43
$\text{MeNH}_2$	116.5	46.7	12.5	3.18	6.50
$\text{H}_2\text{O}$	101.2	39.9	12.0	4.27	7.97
$\text{MeOH}$	109.0	42.6	8.43	3.18	7.09
$\text{Me}_2\text{O}$	110.9	35.2	-2.16	2.63	5.47

<sup>a</sup> The CAM-B3LYP/aug-cc-pVTZ level of theory is used, which has been shown to provide results comparable to CCSD(T) for these systems.<sup>65</sup>

nitrogen ( $\text{NH}_3$  and  $\text{MeNH}_2$ ) than the oxygen-anchoring ones. Despite the larger dipole moment of  $\text{H}_2\text{O}$  vs.  $\text{NH}_3$  (calculated at CAM-B3LYP-aug-cc-pVTZ/experimental values: 1.88/1.85 vs. 1.51/1.47 D),<sup>81</sup> for example, metal-ammonia bonds are more directional. For transition metals, the  $D_e$  values depend also on the electronic state of the metal center. For example, the low-spin Mo complex ( $t_{2g}^5$ ) bears stronger binding to six ammonia ligands than the high spin Fe complex ( $t_{2g}^4e_g^1$ ).<sup>59</sup> Comparison between ammonia and dimethyl-ether complexes of sodium have been also reported in the literature.<sup>82</sup>

Looking at Figure 6, the  $\text{Be}^+ + 4L \rightarrow \text{BeL}_4^+$  binding energies per Be-X bond,  $D_e^{(+)}$ , can be estimated as

$$D_e^{(+)} = D_e^{(2+)} - IE(\text{Be}^+)/4 + IE_2/4,$$

where  $IE(\text{Be}^+)$  and  $IE_2$  are the ionization energies of  $\text{Be}^+$  and  $\text{BeL}_4^+$ ; see Table 1 for  $IE_2$  and  $D_e^{(2+)}$  values. The  $IE(\text{Be}^+)/4$  term is 107.3/105.0 kcal/mol (calculated at CAM-B3LYP with aug-cc-pVTZ/experimental<sup>81</sup>), while the last term contributes between 37 ( $\text{MeNH}_2$ ) and 46 ( $\text{H}_2\text{O}$ ) kcal/mol. Given that  $D_e^{(2+)}$  values are in the 100–120 kcal/mol range, the above terms predict  $D_e^{(+)}$  values  $\sim 60$  kcal/mol lower than  $D_e^{(2+)}$ , which is in perfect agreement with the values of Table 1. In conclusion, the addition of one diffuse electron to  $\text{BeL}_4^{2+}$  destabilizes the complex mainly due to the energy penalty needed to detach the electron from  $\text{Be}^+$ . Along the same lines, the  $\text{Be} + 4X \rightarrow \text{BeX}_4$  binding energies per Be-X bond,  $D_e^{(0)}$ , will be even smaller given as

$$D_e^{(0)} = D_e^{(2+)} - [IE(\text{Be}) + IE(\text{Be}^+)]/4 + [IE_1 + IE_2]/4,$$

where  $IE(\text{Be})$  and  $IE_1$  are the first ionization energies of  $\text{Be}$  and  $\text{BeL}_4$ ; see Table 1 for  $IE_1$ . The contribution of  $IE(\text{Be})$  is 159.8/158.7 (calculated/experimental<sup>81</sup>) and  $IE_1$  is from 56 ( $\text{MeNH}_2$ ) to 71 ( $\text{H}_2\text{O}$ ) kcal/mol resulting in  $D_e^{(0)}$  values of 10–20 kcal/mol.

Another interesting observation is that the coordination of  $\text{MeNH}_2$  to  $\text{Be}^{2+}$  is stronger than  $\text{NH}_3$  with larger  $D_e^{(2+)}$  by 4.7 kcal/mol, but it has lower  $D_e^{(+)}$  and  $D_e^{(0)}$  values by 0.6 and 4.3 kcal/mol, respectively. Since the metal is the same, the difference must be attributed to the last step of the indirect process of Figure 6, meaning that the solvation of electrons is poorer for  $\text{MeNH}_2$  as demonstrated by its  $IE_1$  and  $IE_2$  values (see

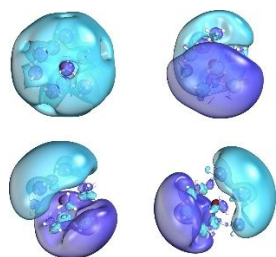


Figure 7. Outer 1s (top left) and the three 1p orbitals of  $\text{Th}(\text{NH}_3)_{10}$ .

Table 1), and this makes SEPs with  $\text{MeNH}_2$  less stable. The same holds true going from  $\text{MeOH}$  to  $\text{Me}_2\text{O}$ ; see Table 1.

Based on the previous discussion, thorium is an excellent candidate for making SEPs with multiple diffuse electrons.<sup>12</sup> For example, thorium has low ionization energies compared to lighter metals, such as titanium (both having a  $s^2d^2$  configuration), and it can host as many as ten ligands (see for example refs. <sup>83, 84</sup>). The first four ionization energies of Th are exceptionally small (6.31, 11.9, 20.0, and 28.8 eV) compared to transition metals and other f-block elements.<sup>81</sup> As a result, thorium can make a  $\text{Th}^{4+}(\text{NH}_3)_{10}$  complex with four peripheral electrons.<sup>12</sup> The geometry of this complex and the occupied outer orbitals ( $1s^22p^2$ ) are shown in Figure 7. It should be mentioned that Eu and Yb ammonia expanded metals have been reported experimentally.<sup>45</sup>

On top of these factors, a separate stability consideration is that of the stability of the ligands within the complex. For example, ammonia and water ligands have been shown to release  $\text{H}_2$ . Two protons ( $\text{H}^+$ ) can combine with two diffuse electrons ( $e^-$ ) to make  $\text{H}_2$ . Therefore  $\text{Be}(\text{NH}_3)_4$ ,  $\text{Be}(\text{MeNH}_2)_4$ ,  $\text{Be}(\text{H}_2\text{O})_4$ , and  $\text{Be}(\text{MeOH})_4$ , will produce  $\text{Be}^{2+}(\text{NH}_3)_2(\text{NH}_2^-)_2$ ,  $\text{Be}^{2+}(\text{MeNH}_2)_2$ ,  $\text{Be}^{2+}(\text{H}_2\text{O})_2(\text{OH}^-)_2$ , and  $\text{Be}^{2+}(\text{MeOH})_2(\text{MeO}^-)_2$ , with no diffuse electrons. The  $\text{H}_2$  release products are more stable than  $\text{BeX}_4$  by 42.6 ( $\text{NH}_3$ ), 59.7 ( $\text{MeNH}_2$ ), 96.7 ( $\text{H}_2\text{O}$ ), and 108.3 ( $\text{MeOH}$ ) kcal/mol (present CAM-B3LYP/aug-cc-pVTZ results). These values compare favorably with the more accurate computational results for  $\text{Be}(\text{NH}_3)_4$  and  $\text{Be}(\text{H}_2\text{O})_4$  of ref. <sup>57</sup> at the CCSD(T)/aug-cc-pVTZ level of theory (39.3 and 94.7 kcal/mol). In addition, according to ref. <sup>57</sup>, the reaction for water is not only more exothermic, but it is also associated with a three times lower energy barrier (8.0 vs. 23.9 kcal/mol). The same barrier for the solvated (in ammonia) dielectrons<sup>85</sup> has been calculated to be 33.4 kcal/mol,<sup>72</sup> while it appears that the barrier and relative energetics can depend strongly on the central metal. For example, the  $\text{H}_2$  release reaction for  $\text{Cr}(\text{NH}_3)_6$  is only slightly exothermic (by 1.8 kcal/mol) and has a barrier of 30.4 kcal/mol, whereas the same values for its second-row transition metal counterpart,  $\text{Mo}(\text{NH}_3)_6$ , are 25.9 and 25.8 kcal/mol.<sup>59</sup> This explains the higher (kinetic) stability of metal ammonia liquid metals. Recently, Jungwirth and co-workers showed that a metal water metallic layer can be observed for several seconds when NaK droplets are exposed to water vapor of  $\sim 10^{-4}$  mbar pressure at room temperature.<sup>16</sup> The continuous provision of electrons from the NaK droplet and water molecules from the

vapor can sustain a quasi-steady-state metallic shell of hundreds of monolayers.

**Computational challenges.** From the technical point of view, a very valid question is what basis functions should be employed for the accurate description of the outer orbitals. For the pseudo-spherical  $\text{Li}(\text{NH}_3)_4$  complex, the use hydrogen-like basis set with a series of diffuse functions located at the center of the complex, i.e. on the metal, is the most sensible choice. Such a basis set for Li is the aug-cc-pVX sequence ( $X = \text{D}, \text{T}, \text{Q}, 5$ ),<sup>86</sup> which includes one diffuse function per angular momentum component. Since more of them may be necessary, we currently started from aug-cc-pVDZ (ADZ) and created the d-aug-cc-pVDZ (DDZ), t-aug-cc-pVDZ (TDZ), and q-aug-cc-pVDZ (QDZ) sets by adding one more diffuse function every time. For each angular momentum, we added a Gaussian-type function with exponent equal to  $1/3$  of the existing smallest exponent, i.e. the exponents for the supplemented s, p, d basis functions of DDZ are  $1/3$  of those in the ADZ, and the same for DDZ $\rightarrow$ TDZ and TDZ $\rightarrow$ QDZ.

On the other hand, the outer electrons are closer to the terminal hydrogen atoms and thus diffuse functions around all H centers may be a better option. To monitor their effect, we used the existing ADZ and DDZ basis sets<sup>87-89</sup> and made the TDZ as we did for Li but dividing by the ratio of the ADZ/DDZ exponents (even-tempered approach). The same approach (adding diffuse functions on terminal hydrogen atoms) has been found more efficient for the study of the molecular Rydberg excited states in difluoromethane.<sup>90</sup>

An important point here is that the used basis functions should not necessarily resemble the Rydberg orbitals of the metal, and further tuning of these exponents can improve the performance of the calculations. Any connection between these basis functions and the Rydberg states of the metal should be avoided or at least stated with extreme caution. In addition, the use of functions centered on the metal can be a poor choice when asymmetric metal complexes are studied, e.g.  $\text{Li}(\text{NH}_3)_4(\text{NH}_3)_2$  [two ligands at one side of the second solvation shell]. The same holds true for the case where the diffuse electrons are away from the metal center, i.e. when two coordination spheres separate the metal from the diffuse electron.<sup>65</sup>

To assess the proper location of the diffuse functions, we made twenty different combinations of double- $\zeta$  quality basis sets with various augmentation schemes (see Table 2) for  $\text{Li}(\text{NH}_3)_4$ . The  $C_{2v}$  symmetry elements were exploited. The notation Li-basis-set/H-basis-set is used from now on. The computational cost of the calculations didn't allow the use of triple- $\zeta$  basis sets, but we find good agreement (within 0.1 eV for excitation energies) when comparing with d-aug-cc-pVTZ (DTZ) results from ref. <sup>58</sup> (see Table 2 and also ref. <sup>65</sup>). The exponents of the diffuse functions in DTZ or quadruple- $\zeta$  basis are of the same order as DDZ.

We obtained the complete basis set (CBS) limit by extrapolating the calculated quantities at the CCSD(T) level towards both dimensions: "infinite" addition of diffuse functions on Li and "infinite" addition of diffuse functions on H. This is not a typical extrapolation of correlation consistent basis sets, since the cardinal number used for each basis set pertains to the degree of augmentation [1 (ADZ), 2 (DDZ), 3 (TDZ), 4 (QDZ)] rather than the size of the valence functions. An

exponential decay was implemented for the various (zero or non-zero external fields) energies. The CBS limits for the

Table 2. CCSD(T) electric properties  $\Theta_{zz}$  and  $\alpha_{zz}$  (a.u.) and excitation energies  $\Delta E$  for the  $1s \rightarrow 1p$  and  $1s \rightarrow 1d$  electronic transitions (eV) of  $\text{Li}(\text{NH}_3)_4$  for various double- $\zeta$  quality Li (Li-bs) and H (H-bs) basis sets combinations.

Li-bs <sup>a</sup>	H-bs <sup>a</sup>	$\Theta_{zz}^b$	$\alpha_{zz}^c$	$\Delta E(1p)^d$	$\Delta E(1d)^e$
DZ	DZ	26.39		0.400	5.220
	ADZ	32.44	1030	0.814	1.837
	DDZ	34.53	1314	0.734	1.480
	TDZ	34.46	1273	0.734	1.479
ADZ	DZ	38.62	1820	0.675	5.027
	ADZ	35.33	1329	0.740	1.863
	DDZ	34.48	1272	0.734	1.481
	TDZ	34.43	1271	0.734	1.480
DDZ	DZ	35.79	1618	0.668	1.763
	ADZ	34.85	1367	0.719	1.800
	DDZ	34.47	1130	0.734	1.480
	TDZ	34.44	1324	0.734	1.479
TDZ	DZ	36.04	1608	0.671	1.380
	ADZ	35.03	1365	0.720	1.467
	DDZ	34.47	1271	0.734	1.478
	TDZ	34.43	1261	0.734	1.478
QDZ	DZ	36.10	1602	0.672	1.381
	ADZ	35.04	1362	0.721	1.467
	DDZ	34.50	1271	0.734	1.478
	TDZ	34.47	1275	0.734	1.478
CBS		34.52	1318	0.734	1.478
DTZ <sup>f</sup>				0.72	1.40

<sup>a</sup> DZ = cc-pVDZ; ADZ = aug-cc-pVDZ; DDZ = d-aug-cc-pVDZ; TDZ = t-aug-cc-pVDZ; QDZ = q-aug-cc-pVDZ; CBS = complete basis set limit extrapolating energies with an exponential expression; see text.

<sup>b</sup> Non-traceless quadrupole moment, calculated by applying finite electric field gradient along the z-axis; see text.

<sup>c</sup> Dipole polarizability, calculated by applying finite electric field along the z-axis; see text. The DZ/DZ calculation had convergence issues at the Hartree-Fock level. The CBS limit is the average of the two CBS approaches described in the text (1299 and 1336 a.u.).

<sup>d</sup> B<sub>1</sub> component.

<sup>e</sup> A<sub>2</sub> component.

<sup>f</sup> CASPT2,P3+/cc-pVTZ(Li,N),d-aug-cc-pVTZ(H).<sup>58</sup>

individual quantities are calculated based on these energy limits (see below).

We used two CBS extrapolation schemes depending on which dimension was extrapolated first. In the first scheme, the DDZ/XDZ, TDZ/XDZ, QDZ/XDZ (X = A, D, T) extrapolations performed first followed by extrapolating these three limits to CBS. In the second scheme, the same process started with XDZ/ADZ, XDZ/DDZ, XDZ/TDZ (X = D, T, Q) extrapolations followed by extrapolating these three limits to CBS. Both schemes gave the exact same values for the significant digits listed in Table 2, except for the dipole polarizability where the average is reported (see footnotes of Table 2).

The quantities we calculated are the first non-vanishing electric moment (quadrupole moment  $\Theta_{zz}$ ) and first non-vanishing polarizability (dipole polarizability  $\alpha_{zz}$ ). The former is the expectation value of  $z^2$  and not of the traceless  $\Theta_{zz}$  corresponding to the  $z^2 - 1/2(x^2 + y^2)$  operator. An electric field

$f$  and an electric field gradient  $g$  of  $10^{-4}$  a.u. were applied (finite field approach), and the two quantities were estimated as:

$$\Theta_{zz} = [E(+g) - E(-g)] / 2g$$

$$a_{zz} = [E(+f) + E(-f) - 2E(0)] / f^2$$

where  $E$  denotes energy and  $\pm$  indicates the direction of the field or field gradient (0 means no external perturbation is present). MOLPRO suite of codes was invoked for these calculations.<sup>91</sup>

Due to the high symmetry ( $T_d$  point group) of the complex,  $\Theta_{zz}$  and  $\alpha_{zz}$  ( $z$  being one of the principal molecular axes) are the only non-zero elements of the corresponding tensors and are equal to the  $xx$  and  $yy$  components. Both are extremely sensitive to the quality of the wavefunction. The obtained  $\Theta_{zz}$  and  $\alpha_{zz}$  values are an order of magnitude larger than values of typical molecules.<sup>81</sup> Our  $\alpha_{zz}$  values are 25% larger than the 986 a.u. value reported earlier in the literature.<sup>46</sup> We also report excitation energies from the 1s to the 1p and 1d outer orbitals.

Overall, the addition of diffuse functions on Li only is not sufficient and convergence to CBS is very slow and, in some cases, not obvious. For example, the results of the XDZ/DZ sequence for  $\Theta_{zz}$  are 38.62, 35.79, 36.04, and 36.10 a.u. vs. the CBS limit of 34.52 a.u. Similar observations can be made for the other quantities. The addition of a series of diffuse functions on H centers (XDZ/ADZ) improves the values considerably, while a second set of diffuse functions (XDZ/DDZ) reaches the CBS limit, even for  $X = A$ . On the other hand, the addition of diffuse functions on H centers leads to CBS values even without the use of diffuse functions on Li, but two sets of diffuse functions are necessary (see DZ/DDZ). Overall, a DDZ set on H centers (with or without diffuse functions on Li) is necessary and sufficient for obtaining CBS-level results. In addition, the utilization of diffuse functions on H centers is a safer choice for non symmetric complexes or when the electrons are displaced far from the metal center.<sup>65</sup>

The metal ammonia species bear higher symmetry, and thus the corresponding peripheral orbitals resemble the hydrogenic orbitals closer. In cases of other ligands or when the solvation shells around the metals are not "isotropic", the symmetry is lower and centric basis functions are not a good choice (see for example ref. <sup>64</sup>).

However, the computational cost for adding diffuse functions on hydrogen centers increases rapidly, mostly because of the large number of terminal hydrogen atoms. Future studies could focus on two directions: Improved central basis functions can be generated, or new basis sets centered on dummy atoms away from the molecular complex and closer to the places where the peripheral electron density is maximum.

As far as the proper methodology is concerned, for species with no prior knowledge multi-reference techniques are initially suggested. Especially for systems with multiple diffuse electrons or systems bearing transition metals. Multi-reference methods are *sine qua non* for excited electronic states.<sup>92</sup> For systems with confirmed single-reference character, like the single radical alkali metal or positively charged alkaline-earth metal ammonia complexes, electron propagator<sup>93</sup> and coupled cluster methodologies are quite beneficial as they can cope with the fine dynamic electron correlation effects and large basis sets.<sup>53</sup> Regarding density functional theory, there is no systematic investigation on proper density functionals, but CAM-B3LYP seems to provide accurate geometries.<sup>65</sup>

**Experimental studies.** Different techniques, such as photoelectron, photodissociation, photoionization, electronic, vibrational, mass spectrometry and depletion spectroscopy have been employed to study lithium, sodium, magnesium, calcium, aluminum, vanadium, chromium, cobalt, nickel, copper, silver ammonia complexes.<sup>20, 32, 94-110</sup>

Regarding, alkali and alkaline earth metals, the binding energy ( $D_0$ ), electron affinity (EA), ionization energy (IE), and excitation energy ( $\Delta E$ ) from the ground to the first excited state have been measured. Specifically,  $D_0[\text{Li}(\text{NH}_3)_4 \rightarrow \text{Li}(\text{NH}_3)_3 + \text{NH}_3] = 3750 \pm 150 \text{ cm}^{-1}$ ,<sup>100</sup>  $\text{EA}(\text{Li}(\text{NH}_3)_4) \approx 0.45 \text{ eV}$ ,<sup>20</sup>  $\text{EA}(\text{Na}(\text{NH}_3)_4) \approx 0.5 \text{ eV}$ ,<sup>20</sup>  $\text{IE}(\text{Li}(\text{NH}_3)_4) \approx 3.025(1) \text{ eV}$ ,<sup>98</sup>  $\Delta E(\text{Li}(\text{NH}_3)_4) \approx 0.8 \text{ eV}$ ,<sup>20</sup>  $0.75 \text{ eV}$ ,<sup>99</sup>  $\Delta E(\text{Na}(\text{NH}_3)_4) \approx 0.7 \text{ eV}$ ,<sup>20</sup>  $0.74 \text{ eV}$ ,<sup>95</sup> and  $\Delta E(\text{Mg}(\text{NH}_3)_{4,5,6}^+) \approx 1.05, 0.99, 0.93 \text{ eV}$ .<sup>97</sup> In all cases  $\Delta E$  pertains to the promotion of one electron from the outer 1s to 1p orbitals, or distorted valence s-to-p metallic orbitals (as mentioned in the literature). Theoretical calculations (CASPT2/d-aug-cc-pVTZ values) are in very good agreement:  $\text{EA}(\text{Li}(\text{NH}_3)_4) = \text{EA}(\text{Na}(\text{NH}_3)_4) = 0.45 \text{ eV}$ ,  $\text{IE}(\text{Li}(\text{NH}_3)_4) = 2.92 \text{ eV}$ ,  $\Delta E(\text{Li}(\text{NH}_3)_4) = 0.72 \text{ eV}$ ,  $\Delta E(\text{Na}(\text{NH}_3)_4) = 0.66 \text{ eV}$ .<sup>58</sup> Finally, the infrared (IR) spectra of neutral calcium-ammonia complexes for various sizes indicate that eight ammonia ligands can coordinate to calcium.<sup>94</sup> A subsequent computational work showed that the formed  $\text{Ca}(\text{NH}_3)_8$  complex hosts two peripheral electrons.<sup>52</sup>

The experimental efforts on transition metal ammonia complexes report primarily IR infrared spectra of mono-cationic species with focus on characterizing their first coordination shell. All of the employed transition metal complexes prefer a tetra-coordinated structure, as indicated by the observed shifts in the N-H stretching frequencies due to hydrogen bonding for larger complexes between first and second solvation shell ammonia molecules. The  $\text{Co}(\text{NH}_3)_4^+$ ,  $\text{Cu}(\text{NH}_3)_4^+$ , and  $\text{Ag}(\text{NH}_3)_4^+$  cations adopt a tetrahedral arrangement,<sup>101-103, 110</sup> whereas  $\text{V}(\text{NH}_3)_4^+$ ,  $\text{Cr}(\text{NH}_3)_4^+$ , and  $\text{Ni}(\text{NH}_3)_4^+$  prefer a less symmetric (planar or seesaw) structure.<sup>59, 96, 101, 104</sup>  $\text{V}(\text{NH}_3)_6^+$  has been predicted computationally as stable structure, and it is possibly higher in energy than  $\text{V}(\text{NH}_3)_4(\text{NH}_3)_2^+$ .<sup>52</sup> In addition, recent theoretical work on chromium and molybdenum ammonia complexes demonstrated that neutral species favor the coordination of more ammonia ligands to the metal and the presence of two peripheral electrons, as happens in calcium ammonia complexes.<sup>59</sup> The same is true switching from first- to second-row transition metals. Future computational and experimental work is necessary to explore the electronic structure of the hitherto unstudied transition metal cationic complexes and their neutral counterparts.

Finally, only one p-block metal has been investigated so far, and specifically the  $\text{Al}(\text{NH}_3)_{1-5}^+$  species.<sup>108</sup> The first shell saturates with four ammonia ligands, while larger species activate one N-H bond of ammonia.

### 3. From Solvated Electron Precursors to Crystalline Materials

As demonstrated above, SEPs share similar electronic structure with atoms, and especially the highly symmetric metal-ammonia complexes. Reasonable follow-up questions are: Can SEP monomers bind together with covalent bonds? Can two  $\text{Li}(\text{NH}_3)_4$  radical

complexes form the analogue of H<sub>2</sub>? Can we make “molecules of molecules”?

Although there is no direct experimental confirmation of dimer formations, it can be implied that Li(NH<sub>3</sub>)<sub>4</sub> start forming dimers at intermediate concentrations in ammonia solutions, oligomers at higher concentrations, and finally a crystal of Li(NH<sub>3</sub>)<sub>4</sub> complexes under saturation conditions (expanded metals). During the formation process (continuous dissolution of metal in ammonia) of expanded metals, hydrogen bonds between ammonia molecules are disrupted<sup>31</sup> and solid expands to accommodate the “free” electrons.<sup>27</sup> Theory suggests that lithium and magnesium are better electron donors than sodium and calcium.<sup>2</sup> Experimentally, the formation process has been explored for both bulk and nanodroplets via photoelectron spectroscopy and nuclear magnetic resonance<sup>111–113</sup> Computationally, the solvation process for Li and Li<sup>-</sup> in ammonia has been studied in the condensed phase and (gas-phase) micro-solvation environments.<sup>114, 115</sup>

It turns out that the H<sub>2</sub>-analogues (SEP contact dimers) are indeed formed. The optimal structure and binding energy for [Li(NH<sub>3</sub>)<sub>4</sub>]<sub>2</sub> and [Na(NH<sub>3</sub>)<sub>4</sub>]<sub>2</sub> have been investigated computationally. First, Zurek *et al.* explored various geometric arrangements for the former showing that the two electrons couple into a single bonding orbital (singlet spin state), and they estimated the binding energy equal to 7.2 kcal/mol.<sup>5</sup> They also studied a tetramer, which has the same “normalized” binding energy (total binding energy divided by the number of SEP monomers). More recently, we found a more stable dimer structure of higher (pseudo-linear) symmetry with binding energy of 15.0 kcal/mol.<sup>58</sup> The sodium species have very similar structure with a longer metal-metal distance and comparable binding energy. In this higher symmetry global minimum, three ammonia ligands of each SEP face each other and one hydrogen

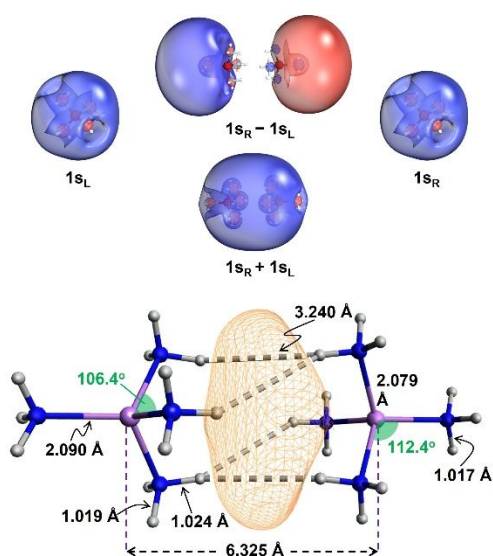


Figure 8. Upper: The combinations of the 1s orbitals of two interacting SEPs form  $\sigma$  ( $= 1s_R + 1s_L$ ) and  $\sigma^*$  ( $= 1s_R - 1s_L$ ) combinations.

Lower: Structure of [Li(NH<sub>3</sub>)<sub>4</sub>]<sub>2</sub> and contour of the electronic density in the middle of the SEP dimer.

atom from each ammonia ligand points to the middle of the SEP dimer (see Figure 8). These H---H contacts have been mentioned in the literature before<sup>5</sup> and they can be attributed to the attraction from the electronic density in the middle of the dimer as happens for the solvated electrons.<sup>24, 116</sup> This picture resembles the first solvation shell of an anionic solute.<sup>117</sup>

The two 1s orbitals of each SEP monomer are combined to make the  $\sigma$  and  $\sigma^*$  orbitals (see Figure 8).<sup>58</sup> The ground state has a  $\sigma^2$  configuration, while the  $\sigma^1\sigma^{*1}$  excited triplet state is only slightly (less than 3 kcal/mol) bound with respect to the two SEP fragments,<sup>5, 58</sup> but certainly it is not repulsive unlike the triplet state of H<sub>2</sub>. The lowest triplet state for [Na(NH<sub>3</sub>)<sub>4</sub>]<sub>2</sub> has actually a  $\sigma^1\pi^1$  electronic configuration (lower by 2 kcal/mol and with a shorter metal-metal bond compared to  $\sigma^1\sigma^{*1}$ ) originating from the combination of a 1s<sup>-</sup>-state Na(NH<sub>3</sub>)<sub>4</sub> and a 1p<sup>-</sup>-state Na(NH<sub>3</sub>)<sub>4</sub>. The same state for [Li(NH<sub>3</sub>)<sub>4</sub>]<sub>2</sub> is practically degenerate with the  $\sigma^1\sigma^{*1}$  state. Overall, two SEP monomers can bind together and create  $\sigma$ ,  $\sigma^*$ ,  $\pi$ , and  $\pi^*$  orbitals as exactly happens for typical diatomic molecules. Similar bonding has been reported between small metal suboxides (Rb<sub>9</sub>O<sub>2</sub>) which also host diffuse outer electrons.<sup>118</sup>

Moving to the condensed phase, the lithium-ammonia expanded or liquid metals can be seen as a three-dimensional grid of Li(NH<sub>3</sub>)<sub>4</sub><sup>+</sup> centers surrounded by a “cloud” of electrons, a Li(NH<sub>3</sub>)<sub>4</sub> polymer, a “superatom of molecular orbitals”,<sup>46</sup> or even electrons provided from Li atoms to the conduction band of ammonia liquid.<sup>119</sup> The latter picture was used to explain the effective electron tunneling in these materials.

These materials have been characterized as metals with the lowest melting point (89 K) known.<sup>120</sup> Three different phases have been identified for the solid state and more recently have been studied in detail with inelastic neutron scattering experiments and computational methods.<sup>46, 120, 121</sup> Edwards and co-workers found that the Li(NH<sub>3</sub>)<sub>4</sub> building units adopt a C<sub>3v</sub> structure (instead of the gas-phase T<sub>d</sub> one), where one lithium-ammonia bond distance is longer and the N-H bonds of this ammonia ligand turn to an eclipsed configuration with respect to the other Li-N bonds.<sup>46</sup> This unexpected arrangement is possibly driven by H---H contacts (see above).<sup>46</sup>

Methylamine-based expanded metals have also attracted a fair amount of interest. As with ammonia, lithium makes tetracoordinate complexes with methylamine. The two kinds of liquid metals demonstrate quite different electric conductivity (methylamine considerably lower),<sup>29</sup> magnetic properties,<sup>25, 26, 28, 30</sup> and even melting points (89 K for ammonia vs. 155 K for methylamine).<sup>30</sup> Their structure has been explored via neutron diffraction experiments,<sup>27, 31</sup> which show that although in ammonia the “free” electrons spread in channels,<sup>31</sup> methylamine makes isolated void spaces.<sup>27</sup> As a result, spin-pairing is less pronounced in methylamine.<sup>28</sup> Interestingly, equimolar mixed ammonia/methylamine solutions have been studied recently yielding highly structured homogeneous species despite the diverse distribution patterns around individual Li<sup>+</sup> ions:

40%  $\text{Li}(\text{NH}_3)_2(\text{CH}_3\text{NH}_2)_2$ , 50%  $\text{Li}(\text{NH}_3)_1(\text{CH}_3\text{NH}_2)_3$  or  $\text{Li}(\text{NH}_3)_3(\text{CH}_3\text{NH}_2)_1$ , and 10%  $\text{Li}(\text{NH}_3)_4$  or  $\text{Li}(\text{CH}_3\text{NH}_2)_4$ .<sup>29</sup>

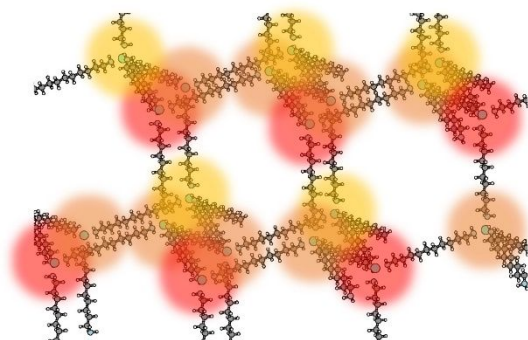


Figure 9. Crystal structure of the recently proposed lithium linked-SEPs. The blur spheres represent peripheral electrons.

In the above materials, there is a grid of disconnected positively charged metal complexes surrounded by weakly bound (“free”) electrons. A recently proposed system is offered through the use of diamines to link two SEP species together.<sup>47</sup> From this, one can make MOF-type (MOF=metal-organic-framework) materials composed of metal centers with diffuse peripheral electrons. The first system of this type to be studied consists of lithium-diamine-lithium bridges in a diamond-like arrangement (see Figure 9).<sup>47</sup> The electronic structure of these systems has been studied theoretically and shown that it depends on the length of the diamine linker. Short hydrocarbon backbones favor metallic behavior (similar to unbridged SEPs/expanded metals), while longer ones bear small band gaps pointing to semiconducting behavior.<sup>47</sup>

Going into more detail, a linked-SEP with two lithium centers, such as  $(\text{NH}_3)_3\text{Li}-\text{NH}_2(\text{CH}_2)_n\text{H}_2\text{N}-\text{Li}(\text{NH}_3)_3$  with  $n=1-10$ ,<sup>47</sup> can also be viewed as two H atoms kept fixed at a specific distance defined by  $n$ . Therefore, the two remote electrons in the case of  $n=10$  couple into degenerate triplet and singlet states. As  $n$  drops, the singlet-triplet gap increases since in the singlet state the two electrons form a  $\sigma$  bonding orbital as happens for  $[\text{Li}(\text{NH}_3)_4]_2$ .<sup>47</sup> The transition from the open-shell singlet ( $n=10$ ) to the closed-shell singlet ( $n=1$ ) is only described properly with multi-configurational wavefunctions, which poses doubts about the performance of density functional theory applied in the condensed phase calculations for intermediate  $n$  values.<sup>47</sup> In addition to the pseudo-linear  $(\text{NH}_3)_3\text{Li}-\text{NH}_2(\text{CH}_2)_n\text{H}_2\text{N}-\text{Li}(\text{NH}_3)_3$  structures, curved or “circular” structures were also identified, where the hydrocarbon chain bends to allow the direct contact of the two terminal electrons. The two kinds of structures are competitive within 5 kcal/mol. Similar electronic structure has been reported for the non-metallic species  $(\text{NH}_3)(\text{CH}_2)_n(\text{NH}_3)$ , where the two terminal N atoms are positively charged and can host two diffuse electrons.<sup>122</sup> The latter species can be seen as the “dimers” of  $\text{NH}_4$  radicals.<sup>123-125</sup>

Given that the metal-ammonia, metal-methylamine, or metal-diamine bonds are weak (of the order of 10 kcal/mol), the thermal stability of the linked dimers or MOF-type materials is of concern as these bonds can dissociate at moderate temperature values. In addition, diamines can make chelate complexes.<sup>64</sup> Future molecular

dynamics simulations will provide more accurate answers, but the idea of replacing the metal-nitrogen coordinative bonds with metal-carbon covalent bonds has appeared in the literature.<sup>126, 127</sup>

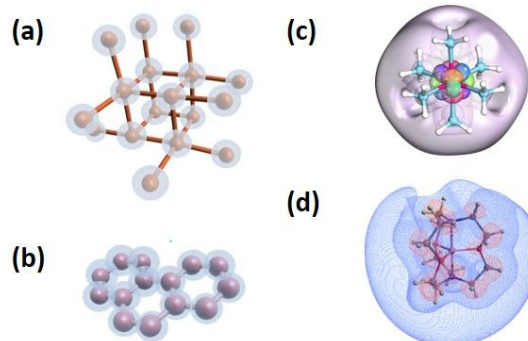


Figure 10. Proposed linked-SEP structures for future studies: MOF-type (a) and graphene-type (b) arrangements composed of polydentate s-, d- or f-block metal complexes. A transition metal center with its inner and outer electrons (c) and an alkali metal cryptand (d) are shown as representative units.

Specifically, we recently studied  $(\text{NH}_3)_3\text{Be}-\text{CH}_2(\text{CH}_2)_n\text{H}_2\text{C}-\text{Be}(\text{NH}_3)_3$  and  $(\text{NH}_3)_3\text{B}-\text{CH}_2(\text{CH}_2)_n\text{H}_2\text{C}-\text{B}(\text{NH}_3)_3$  with one and two outer electrons per terminus, respectively.<sup>126, 127</sup> Therefore, the former is still analogue of  $\text{H}_2$ , but the latter is analogue of  $\text{He}_2$ . The replacement of Li with Be is necessary, since one metallic electron is dedicated for the formation of the covalent bond with carbon. At the same time, the replacement of the NH bonds with CH isolates the diffuse electrons of the two termini by “pushing” them away from the inter-SEP space. As a result the coupling of the two electrons in a closed-shell singlet occurs only at very short hydrocarbon chains for Be (as evidenced by the abrupt change from  $n=2$  to  $n=1$  for Be-C and gradual change from  $n=4$  to  $n=1$  for Li-N combinations).<sup>47, 126</sup>

To sum up, starting from the metal ammonia building units, two different types of materials have been reported in the literature. The first is the experimentally characterized expanded or liquid metals are aggregates of SEP complexes. The second arises from tethering adjacent SEPs via hydrocarbon chains leads to more structured materials with various possible topologies, such as diamond-like, graphene-like, or MOF-like. Decoration of linkers with polar or conjugated groups is expected to enhance the “communication” between electrons of neighboring SEPs, whereas non-polar bulky units will act as insulators for these electrons. Covalent bonds between the linkers and metals will add to the stability of these materials.

An important point of caution pertains to the computational challenges for these crystalline materials. It has been shown recently that the commonly used density functional theory calculations under periodic boundary conditions can severely fail in describing the spin coupling of neighboring diffuse electrons.<sup>47</sup> Since multi-configurational methods for periodically repeated systems (necessary in such cases) are not currently available or practical, density functional theory calculations should be used with caution.

Since every such bond “consumes” one diffuse electron, SEPs with multiple diffuse electrons, such as  $\text{Th}(\text{NH}_3)_{10}$ , are to be used so that diffuse electrons are still have available after the formation of

the bonds. Alternatively, multi-dentate ligands, such as cryptands or aza-crowns, can be used to increase the thermal stability of the metal-ligand bonds.<sup>10</sup> Figure 10 summarizes proposed future

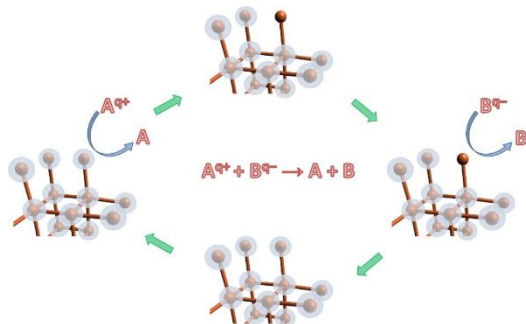


Figure 11. Proposed catalytic cycle for redox reactions using linked-SEP materials ( $q$  can be larger than 1).

strategies to obtain stable materials with diffuse electrons and controlled properties/features.

For both linked-SEPs and expanded metals, a valid concern is the thermal instability, i.e. increased temperature can lead to the dissociation of the relatively weak metal-nitrogen bonds, and need special conditions to avoid reaction with air. For the first concern, the replacement of diamines with cryptands or poly-dentate amine ligands is necessary,<sup>11</sup> while more studies focusing primarily on the reactivity of SEPs with  $N_2$  and  $O_2$  will be helpful. For applications, such as quantum computing (see below), these should not be a concern since they operate at cryogenic air-free environments.

Also, it will be interesting to mix SEPs of different metals for both linked-SEPs and expanded metals and see how this will affect the electronic features and chemical activity of these materials. Another possibility is the formation of SEP oligomers/nanoparticles similar to superatoms (see features and perspectives of such materials in ref. <sup>128</sup>).

Finally, an interesting aspect is the role of solvent molecules close to metal surfaces or electrodes which can serve as an electron source.<sup>129</sup> Can metal-ammonia complexes from the solution borrow electrons at the metal-solvent interface? And what will this mean for the electron transport properties? What happens at liquid/liquid interfaces? The formation of a liquid metal layer between a conventional metal and a solution could offer a way to adjust reduction or oxidation potentials.

#### 4. Possible applications

**Redox catalysis.** Solvated electrons in ammonia have long been used for reduction of aromatic rings (Birch reduction).<sup>130, 131</sup> The reduction power of solvated electrons in either ammonia, water, or ethanol has been utilized for  $CO_2$ ,  $O_2$ ,  $N_2$ ,  $NO$ ,  $N_2O$ ,  $NO_3^-$ ,  $CH_3CN$ , and esters (Bouveault–Blanc reduction).<sup>132–141</sup> Dissolving calcium as a source of solvated electrons in ammonia has been shown to have higher selectivity towards various organic compounds.<sup>142</sup>

It is rather straightforward that the diffuse electrons in expanded metals or peripheral electrons of linked-SEPs can be exploited for reduction reactions.<sup>48</sup> Compared to solvated electrons, SEPs turn positively charged after offering an electron, which can in

principle request the missing electron back. For example, the transfer of an electron to  $CO_2$  converts it to radical species which can react with possibly  $H_2$ ,  $H_2C=CH_2$ , or other substrates. The former make  $H_2C(OH)_2$  [or  $H_2C=O + H_2O$ ] and the latter initiates a radical polymerization mechanism.<sup>48</sup> The return of an electron back to the positively charged SEP center can close the redox catalytic cycle (see Figure 11). Although theory provides a proof of principle for this redox catalysis reactivity,<sup>48</sup> more work (both theoretical and experimental) to this direction is necessary for practical applications.

Another benefit of using SEPs instead of solvated electrons is that the *in situ* created positive charge facilitates the formation of genuinely unstable anions. For example,  $CO_2$  has negative electron affinity in the gas phase ( $CO_2^-$  is unstable), but its interaction with the *in situ* produced  $Li(NH_3)_4^+$  leads to products [ $Li(NH_3)_4^+ CO_2^-$ ] nearly 20 kcal/mol lower in energy than the  $Li(NH_3)_4 + CO_2$  reactants; the activation barrier for this reaction is negligible.<sup>48</sup> Therefore, the presented materials are expected to enable the reduction of species with highly unstable anions.

Furthermore, we can replace Li with alkaline earth, transition, or f-block metals, which can host more than one peripheral electron. As a result, this could enable two-, three-, or even four-electron reductions in a single step. This observation can open the avenue for addressing long-standing chemistry enigmas and revealing novel synthetic routes.

Looking specifically at linked-SEPs, another interesting aspect is how the periodicity affects the chemical activity of these materials. Do the SEP centers act as independent and isolated systems or do the periodic conditions and correlation of electronic neighbors impose a kind of collective or long-range behavior? The isolated behavior is expected for linkers with long chains, but it is unclear how linked-SEPs with shorter chains will behave. Future calculations are necessary for shedding light on this topic. The metal centers in MOFs act as isolated entities, but the diffuse nature of the electrons in linked-SPEs can change this. Finally, the pore size of these materials will be controlled by the length and identity of the linker chain. As such, tuning of pore size may offer selectivity to control the size and polarity of molecules able to diffuse within the material. Concerning expanded metals, they are expected to act as a sort of electrodes, and it remains to see how many electrons can be provided to approaching substrates and if substrates can cross the low-density surface and “dive in the sea of electrons”.

**Electronic devices.** As discussed above, the band structure of lithium-based linked-SEPs depends on the linker’s length (metal for short chains / semiconductor for longer chains). Facilitating or blocking the “communication” between electrons of adjacent SEPs (see above), the band gap can change considerably. Polar groups are expected to facilitate the delocalization of the electrons increasing the metallic character, while bulky hydrocarbon side chains will isolate the electrons further pushing the materials towards the insulators regime.

Employing transition metals instead of Li or other s-block metals, the discussion in the previous section suggests that there will be additional inner *d*-electrons well-separated from the outer diffuse

electrons (two per SEP center; see Figure 12). As a result, the electronic band structure pertaining to the diffuse electrons is expected to remain nearly unaffected: the 1s-band will be separated

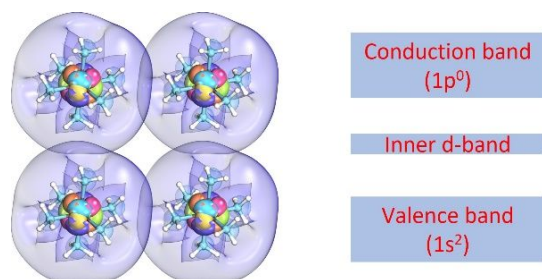


Figure 12. Left: Contours of the inner and outer electrons in a *d*-block expanded metal material. Right: Rough diagram of the expected band structure.

from the 1p-band. Somewhere, between them there will be a “thin” band corresponding to the inner *d*-electrons. The scheme for expected band structure is shown in Figure 12. The actual electronic band structure and the relative positions of the three involved bands can be provided by quantum mechanical calculations, and will define the electronic properties of these materials, which may depend on the metal identity.

Based on the structure and discussion of Section 3, the structure of *d*-metal SEPs will be different from the structure of the  $M(\text{NH}_3)_6\text{X}_2$  crystals [ $M = \text{V}, \text{Cr}, \text{Mn}, \text{Fe}, \text{Co}, \text{Ni}$ ;  $\text{X} = \text{Cl}, \text{Br}, \text{I}$ ]<sup>143</sup> in the sense that the orientation of the  $M(\text{NH}_3)_6^{2+}$  prisms will be determined by the created H---H contacts.

**Quantum computing, sensing, and optics.** Quantum computing is based on the information that can be stored and processed by a molecular or atomic system in synergy with photons in the form of a qubit. Compared to conventional computing systems, quantum computers will be able to outperform in terms of data processing speed. In the simplest model a qubit is represented by a two-level system of nearly degenerate states and the information is encrypted within the wavefunction of the system, which is a superposition of two states. The spin of a single electron within some magnetic field can serve for this purpose.<sup>144-148</sup> For high-quality qubits, the coherence of the wavefunction over time is important and has to be persistent at least as long as the qubit is processed, for instance, while a quantum gate operates. Another aspect is the correlation of two or more neighboring qubits (quantum entanglement) and the degree this can be controlled. Quantum decoherence and controlled entanglement are two common concerns. In addition, the qubits should be easily set to an initial value and should be easily read. Although there is some success for small quantum systems,<sup>149</sup> scalability to larger systems is a major bottleneck.<sup>150</sup>

Ion traps and optical tweezers have been used to create arrays of charged and neutral atoms to be used as qubits. Ultra-cold conditions are necessary to avoid atoms escaping the trap and minimize the loss of information (noise) due to the thermal motion. A different arrangement of qubits can be realized with molecular complexes<sup>144, 151-153</sup> and solid state materials, such as MOFs by

selecting proper metal/linker combinations<sup>154,155</sup> or two-dimensional polymer species.<sup>156</sup> An unpaired electron at each metal center can be used as qubit, while quantum gates can be realized by involving a “third-party” spin.<sup>157</sup> MOF-type species offer high tenability via structural and electronic structure modifications,<sup>158</sup> but the proposed polymers have the benefit of avoiding *d*-electrons and spin-orbit effects, which interfere with the coherence of the spin qubits.<sup>156</sup>

Recently, the use of Rydberg atomic states as qubits has been considered advantageous.<sup>159-161</sup> Fundamentally, the Rydberg states resemble a hydrogen atom and thus “physicists have a straightforward model to help guide intuition”.<sup>161</sup> In addition, the diffuse nature of the electrons (large polarizabilities) enable strong long-range interactions with neighboring atoms (important for two-qubit gate entanglement),<sup>159</sup> Rydberg states have relatively large life times, can form easier large arrays of qubits (scalability), and can be tuned with multiple ways (static or optical electric fields). The major limitation of utilizing Rydberg states is their finite lifetime and off-resonant excitations to unwanted Rydberg states.<sup>159, 162, 163</sup>

The linked-SEPs seem a promising material that combine the advantages of all above materials (molecular and Rydberg qubits) and can also bypass the lifetime limitations of Rydberg excited states as the diffuse 1s-type electron pertains to the ground state of the system. The electronic spectrum of SEPs resembles that of a typical hydrogenic model offering *a priori* fundamental understanding/prediction of their properties. For example, the transition dipole moment between the ground state (1s) and first excited state (1p) is very large as happens to the atomic  $s \rightarrow p$  transitions (see previous sections). The unpaired electron (exposed in a magnetic field) in the 1s orbital can be used to create the two-state qubit. The  $1s \rightarrow 1p$  transition can be used for initialization and measurement of the qubits. Entanglement with neighboring SEPs can be tuned by changing the length and type of the linker. For example, the singlet-triplet splitting (used here to gauge this interaction) for two neighboring electrons ranges from 0 (long chains) to 800  $\text{cm}^{-1}$  (short chains).<sup>47</sup> A more ambitious application would be the design of a photo-sensitive linker that changes conformation upon receiving light similarly to MOF materials.<sup>164</sup> This geometry change of the linker can potentially act as a quantum gate by switching on and off the interaction of qubits. Similar approaches are proposed for MOF-type materials.<sup>165</sup> Also, the qubits are physically tethered via molecular linkers and there is no need for optical or ion traps.

On a different note, the high polarizability of SEPs (see above and ref. 46) makes them very sensitive to the ambient electric fields, and thus excellent quantum sensors. The perturbation for the 1s orbital can be ideally measured via the  $1s \rightarrow 1p$  excitation or the vibrational frequency of the N–H bonds. As an indication, the harmonic vibrational frequency of the N–H bonds drops by 75  $\text{cm}^{-1}$  going from  $\text{Li}(\text{NH}_3)_4^+$  to  $\text{Li}(\text{NH}_3)_4$ , and by 17  $\text{cm}^{-1}$  going from  $\text{Li}(\text{NH}_3)_4$  to  $\text{Li}(\text{NH}_3)_4^-$  (see SI of ref. 58). The same numbers for sodium-ammonia analogue are 67 and 18  $\text{cm}^{-1}$  showing a kind of universal behavior. Calculations of the  $1s \rightarrow 1p$  excitation energies and the N–H frequencies for various electric fields will shed more light on this topic.

Finally, due to their similarity to Rydberg atoms, SEP-based materials can be also used for non-linear quantum optics.<sup>163</sup> Older studies in optical properties of lithium/sodium-ammonia solutions and calcium-ammonia solutions revealed considerably different dielectric constants for alkali and alkaline earth metals.<sup>166</sup> This observation suggests that the study of optical properties for various types of metals is essential.

Based on the above discussions, the utilization of linked SEPs as quantum information systems is a new totally unexplored avenue. Synthesis of these materials will provide valuable input for the future of the present ideas. In the meantime, theoretical calculations should continue to shed light and try to identify ideal candidate structures. For the accurate description of the wavefunction for these open shell-systems bearing diffuse electrons, one is required to apply methods which include both static and dynamic electron correlation combined with large basis sets.<sup>167</sup>

## 5. Conclusions and Outlook

This perspective reviews the unique electronic structure features of metal ammonia complexes and their condensed phase analogues (expanded metals). For all types of metals in the periodic table, the ammonia complexes are shown to host peripheral electrons, which populate a hydrogenic shell model. The observed shell model is universal and resembles that of the Jellium model. In addition to the outer electrons, transition metals also bear inner d-electrons, while f-block metals can accommodate more diffuse electrons. These species mimic atoms and make chemical bonds to form aggregates. In a different direction, theory predicted that new materials, where metal ammonia complexes are tethered with hydrocarbon chains, make them promising candidates for reduction-oxidation chemical reactions and quantum information technology. Experimental assessment of the theory findings is essential for future uses of the proposed materials from both the gas- and condensed-phase experiments.

## Conflicts of interest

There are no conflicts to declare.

## Acknowledgements

The authors are indebted to Auburn University for financial support and especially the James E. Land endowment. This work was completed with resources provided by the Auburn University Easley Cluster. This material is based upon work supported by the National Science Foundation under Grant No. CHE-1940456.

## Notes and references

- B. A. Jackson, J. Harshman and E. Miliordos, *J. Chem. Educ.*, 2020, **97**, 3638-3646.
- V. V. Chaban and O. V. Prezhdo, *J. Phys. Chem. B*, 2016, **120**, 2500-2506.
- E. Miliordos, *Phys. Rev. A*, 2010, **82**, 062118.
- M. Reiher and A. Hirsch, *Chem. Eur. J.*, 2003, **9**, 5442-5452.
- E. Zurek, P. P. Edwards and R. Hoffmann, *Angew. Chem. Int. Ed.*, 2009, **48**, 8198-8232.
- C. Liu, S. A. Nikolaev, W. Ren and L. A. Burton, *J. Mater. Chem. C*, 2020, **8**, 10551-10567.
- J. L. Dye, *Science*, 2003, **301**, 607.
- S. B. Dawes, D. L. Ward, R. H. Huang and J. L. Dye, *J. Am. Chem. Soc.*, 1986, **108**, 3534-3535.
- A. Ellaboudy, J. L. Dye and P. B. Smith, *J. Am. Chem. Soc.*, 1983, **105**, 6490-6491.
- M. Y. Redko, J. E. Jackson, R. H. Huang and J. L. Dye, *J. Am. Chem. Soc.*, 2005, **127**, 12416-12422.
- I. R. Ariyaratna, *Inorg. Chem.*, 2022, **61**, 579-585.
- Z. Lu, B. A. Jackson and E. Miliordos, *Molecules*, 2023, **28**, 4712.
- Y. Zhang, Z. Xiao, T. Kamiya and H. Hosono, *J. Phys. Chem. Lett.*, 2015, **6**, 4966-4971.
- Y. Tsuji, W. Hashimoto and K. Yoshizawa, *Bull. Chem. Soc. Jpn.*, 2019, **92**, 1154-1169.
- T. A. Kaplan, J. F. Harrison, J. L. Dye and R. Rencsok, *Phys. Rev. Lett.*, 1995, **75**, 978-978.
- P. E. Mason, H. C. Schewe, T. Buttersack, V. Kostal, M. Vitek, R. S. McMullen, H. Ali, F. Trinter, C. Lee, D. M. Neumark, S. Thürmer, R. Seidel, B. Winter, S. E. Bradforth and P. Jungwirth, *Nature*, 2021, **595**, 673-676.
- C. Berg, U. Achatz, M. Beyer, S. Joos, G. Albert, T. Schindler, G. Niedner-Schatteburg and V. E. Bondybey, *Int. J. Mass Spectrom. Ion Proc.*, 1997, **167-168**, 723-734.
- A. C. Harms, S. N. Khanna, B. Chen and A. W. Castleman, *J. Chem. Phys.*, 1994, **100**, 3540-3544.
- B. M. Reinhard and G. Niedner-Schatteburg, *Physical Chemistry Chemical Physics*, 2002, **4**, 1471-1477.
- R. Takasu, F. Misaizu, K. Hashimoto and K. Fuke, *J. Phys. Chem. A*, 1997, **101**, 3078-3087.
- J. V. Barnes, B. L. Yoder and R. Signorell, *J. Phys. Chem. A*, 2019, **123**, 2379-2386.
- A. H. C. West, B. L. Yoder, D. Luckhaus, C.-M. Saak, M. Doppelbauer and R. Signorell, *J. Phys. Chem. Lett.*, 2015, **6**, 1487-1492.
- L. Mones, G. Pohl and L. Turi, *Phys. Chem. Chem. Phys.*, 2018, **20**, 28741-28750.
- J. A. Walker and D. M. Bartels, *J. Phys. Chem. A*, 2016, **120**, 7240-7247.
- P. P. Edwards, A. R. Lusic and M. J. Sienko, *J. Chem. Phys.*, 1980, **72**, 3103-3112.
- R. Hagedorn and M. J. Sienko, *J. Phys. Chem.*, 1982, **86**, 2094-2097.
- S. Hayama, J. C. Wasse, N. T. Skipper and A. K. Soper, *J. Phys. Chem. B*, 2002, **106**, 11-14.
- Y. Nakamura, M. Niibe and M. Shimoji, *J. Phys. Chem.*, 1984, **88**, 3755-3760.
- A. G. Seel, H. Swan, D. T. Bowron, J. C. Wasse, T. Weller, P. P. Edwards, C. A. Howard and N. T. Skipper, *Angew. Chem. Int. Ed.*, 2017, **56**, 1561-1565.
- A. M. Stacy, D. C. Johnson and M. J. Sienko, *J. Chem. Phys.*, 1982, **76**, 4248-4254.
- H. Thompson, J. C. Wasse, N. T. Skipper, S. Hayama, D. T. Bowron and A. K. Soper, *J. Am. Chem. Soc.*, 2003, **125**, 2572-2581.
- E. H. Alsharaeh, *Int. J. Mol. Sci.*, 2011, **12**, 9095-9107.

33. N. Gremmo and J. E. B. Randles, *J. Chem. Soc., Faraday Trans. 1*, 1974, **70**, 1480-1487.
34. P. J. M. van Andel, A. H. Wonders and E. Barendrecht, *J. electroanal. chem. interfacial electrochem.*, 1991, **301**, 87-100.
35. H. Dong, Y. Feng and Y. Bu, *J. Phys. Chem. A*, 2023, **127**, 1402-1412.
36. Q. Zheng, T. Feng, J. A. Hachtel, R. Ishikawa, Y. Cheng, L. Daemen, J. Xing, J. C. Idrobo, J. Yan, N. Shibata, Y. Ikuhara, B. C. Sales, S. T. Pantelides and M. Chi, *Sci. Adv.*, **7**, eabe6819.
37. H. Hosono and M. Kitano, *Chem. Rev.*, 2021, **121**, 3121-3185.
38. H. Buchhammagari, Y. Toda, M. Hirano, H. Hosono, D. Takeuchi and K. Osakada, *Org. Lett.*, 2007, **9**, 4287-4289.
39. M. Kitano, Y. Inoue, Y. Yamazaki, F. Hayashi, S. Kanbara, S. Matsuishi, T. Yokoyama, S.-W. Kim, M. Hara and H. Hosono, *Nat. Chem.*, 2012, **4**, 934-940.
40. Y. Kobayashi, M. Kitano, S. Kawamura, T. Yokoyama and H. Hosono, *Catal. Sci. Technol.*, 2017, **7**, 47-50.
41. Y. Toda, H. Hirayama, N. Kuganathan, A. Torrisi, P. V. Sushko and H. Hosono, *Nat. Comm.*, 2013, **4**, 2378.
42. T.-N. Ye, J. Li, M. Kitano, M. Sasase and H. Hosono, *Chem. Sci.*, 2016, **7**, 5969-5975.
43. W. H. J. Brendley and E. C. Evers, in *Solvated Electron*, AMERICAN CHEMICAL SOCIETY, 1965, vol. 50, ch. 9, pp. 111-124.
44. F. Leclercq, P. Damay, A. J. Dianoux and W. Press, Berlin, Heidelberg, 1987.
45. W. S. Glaunsinger, R. B. Von Dreele, R. F. Marzke, R. C. Hanson, P. Chieux, P. Damay and R. Catterall, *J. Phys. Chem.*, 1984, **88**, 3860-3877.
46. A. G. Seel, E. Zurek, A. J. Ramirez-Cuesta, K. R. Ryan, M. T. J. Lodge and P. P. Edwards, *Chem. Comm.*, 2014, **50**, 10778-10781.
47. B. A. Jackson, S. G. Dale, M. Camarasa-Gómez and E. Miliordos, *J. Phys. Chem. C*, 2023, **127**, 9295.
48. B. A. Jackson and E. Miliordos, *Chem. Comm.*, 2022, **58**, 1310-1313.
49. G. W. T. M. J. Frisch, H. B. Schlegel, G. E. Scuseria, M. A. Robb, J. R. Cheeseman, G. Scalmani, V. Barone, G. A. Petersson, H. Nakatsuji, X. Li, M. Caricato, A. V. Marenich, J. Bloino, B. G. Janesko, R. Gomperts, B. Mennucci, H. P. Hratchian, J. V. Ortiz, A. F. Izmaylov, J. L. Sonnenberg, D. Williams-Young, F. Ding, F. Lipparini, F. Egidi, J. Goings, B. Peng, A. Petrone, T. Henderson, D. Ranasinghe, V. G. Zakrzewski, J. Gao, N. Rega, G. Zheng, W. Liang, M. Hada, M. Ehara, K. Toyota, R. Fukuda, J. Hasegawa, M. Ishida, T. Nakajima, Y. Honda, O. Kitao, H. Nakai, T. Vreven, K. Throssell, J. A. Montgomery, Jr., J. E. Peralta, F. Ogliaro, M. J. Bearpark, J. J. Heyd, E. N. Brothers, K. N. Kudin, V. N. Staroverov, T. A. Keith, R. Kobayashi, J. Normand, K. Raghavachari, A. P. Rendell, J. C. Burant, S. S. Iyengar, J. Tomasi, M. Cossi, J. M. Millam, M. Klene, C. Adamo, R. Cammi, J. W. Ochterski, R. L. Martin, K. Morokuma, O. Farkas, J. B. Foresman, and D. J. Fox, Gaussian 16, Revision A.03, Gaussian, Inc., Wallingford CT, 2016.
50. T. Sommerfeld and K. M. Dreux, *J. Chem. Phys.*, 2012, **137**, 244302.
51. B. Baranyi and L. Turi, *J. Chem. Phys.*, 2019, **151**, 204304.
52. I. R. Ariyaratna, N. M. S. Almeida and E. Miliordos, *J. Phys. Chem. A*, 2019, **123**, 6744-6750.
53. I. R. Ariyaratna, S. N. Khan, F. Pawłowski, J. V. Ortiz and E. Miliordos, *J. Phys. Chem. Lett.*, 2018, **9**, 84-88.
54. A. M. Champsaur, A. Velian, D. W. Paley, B. Choi, X. Roy, M. L. Steigerwald and C. Nuckolls, *Nano Lett.*, 2016, **16**, 5273-5277.
55. A. Tlahuice-Flores and A. Muñoz-Castro, *Int. J. Quantum Chem.*, 2019, **119**, e25756.
56. N. M. S. Almeida and E. Miliordos, *Phys. Chem. Chem. Phys.*, 2019, **21**, 7098-7104.
57. I. R. Ariyaratna and E. Miliordos, *Phys. Chem. Chem. Phys.*, 2019, **21**, 15861-15870.
58. I. R. Ariyaratna, F. Pawłowski, J. V. Ortiz and E. Miliordos, *Phys. Chem. Chem. Phys.*, 2018, **20**, 24186-24191.
59. B. A. Jackson and E. Miliordos, *J. Chem. Phys.*, 2021, **155**, 014303.
60. I. R. Ariyaratna and E. Miliordos, *Phys. Chem. Chem. Phys.*, 2020, **22**, 22426-22435.
61. P. Jena and Q. Sun, *Chem. Rev.*, 2018, **118**, 5755-5870.
62. Z. Luo and A. W. Castleman, *Acc. Chem. Res.*, 2014, **47**, 2931-2940.
63. J. W. Rohl, *Modern Physics from alpha to Z0*, 1994.
64. I. R. Ariyaratna and E. Miliordos, *Phys. Chem. Chem. Phys.*, 2021, **23**, 20298-20306.
65. I. R. Ariyaratna, F. Pawłowski, J. V. Ortiz and E. Miliordos, *J. Phys. Chem. A*, 2020, **124**, 505-512.
66. S. N. Khan and E. Miliordos, *J. Phys. Chem. A*, 2020, **124**, 4400-4412.
67. A. Kramida, Ralchenko, Yu., Reader, J., and NIST ASD Team (2019). NIST Atomic Spectra Database (ver. 5.7.1), [Online]. Available: <https://physics.nist.gov/asd> [2020, October 11]. National Institute of Standards and Technology, Gaithersburg, MD. DOI: <https://doi.org/10.18434/T4W30F>.
68. C. I. León-Pimentel, H. Saint-Martin and A. Ramírez-Solís, *J. Phys. Chem. A*, 2023, DOI: 10.1021/acs.jpca.2c08432.
69. A. Hattab, Z. Dhaouadi, A. Malloum, J. J. Fifen, S. Lahmar, N. Russo and E. Sicilia, *J. Comput. Chem.*, 2019, **40**, 1707-1717.
70. R. Shannon, *Acta Crystallogr. A*, 1976, **32**, 751-767.
71. I. R. Ariyaratna and E. Miliordos, *Int. J. Quantum Chem.*, 2018, **118**, e25673.
72. M. Mauksch and S. B. Tsogoeva, *Phys. Chem. Chem. Phys.*, 2018, **20**, 27740-27744.
73. B. M. Reinhard and G. Niedner-Schatteburg, *Phys. Chem. Chem. Phys.*, 2002, **4**, 1471-1477.
74. J. L. Dye, *Angew. Chem. Int. Ed.*, 1979, **18**, 587-598.
75. J. L. Dye, J. M. Ceraso, M. T. Lok, B. L. Barnett and F. J. Tehan, *J. Am. Chem. Soc.*, 1974, **96**, 608-609.
76. I. R. Ariyaratna, *Int. J. Quantum Chem.*, 2021, **121**, e26774.
77. M. Díaz-Tinoco and J. V. Ortiz, *J. Chem. Phys.*, 2019, **151**, 054301.
78. E. Opoku, F. Pawłowski and J. V. Ortiz, *J. Chem. Phys.*, 2021, **154**, 234304.
79. M. Díaz-Tinoco and J. V. Ortiz, *J. Phys. Chem. A*, 2019, **123**, 10961-10967.
80. E. Opoku, F. Pawłowski and J. V. Ortiz, *Phys. Chem. Chem. Phys.*, 2022, **24**, 18347-18360.
81. W. M. Haynes, *CRC Handbook of Chemistry and Physics, 93rd Edition*, Taylor & Francis, 2012.
82. A. O. Gunina and A. I. Krylov, *J. Phys. Chem. A*, 2016, **120**, 9841-9856.
83. F. Blanchard, M. Rivenet, N. Vigier, I. Hablot, S. Grandjean and F. Abraham, *Cryst. Growth Des.*, 2018, **18**, 4593-4601.
84. C. D. Tutson and A. E. V. Gorden, *Coord. Chem. Rev.*, 2017, **333**, 27-43.
85. G. J. Martyna, Z. Deng and M. L. Klein, *J. Chem. Phys.*, 1993, **98**, 555-563.
86. B. P. Prascher, D. E. Woon, K. A. Peterson, T. H. Dunning and A. K. Wilson, *Theor. Chem. Acc.*, 2011, **128**, 69-82.

87. T. H. Dunning, *J. Chem. Phys.*, 1989, **90**, 1007-1023.
88. R. A. Kendall, T. H. Dunning and R. J. Harrison, *J. Chem. Phys.*, 1992, **96**, 6796-6806.
89. D. E. Woon and T. H. Dunning, *J. Chem. Phys.*, 1994, **100**, 2975-2988.
90. M. H. Palmer, S. Vrønning Hoffmann, N. C. Jones, M. Coreno, M. de Simone and C. Grazioli, *J. Chem. Phys.*, 2018, **148**, 214304.
91. H.-J. Werner, P. J. Knowles, G. Knizia, F. R. Manby, M. {Schütz}, P. Celani, W. Györffy, D. Kats, T. Korona, R. Lindh, A. Mitrushenkov, G. Rauhut, K. R. Shamasundar, T. B. Adler, R. D. Amos, A. Bernhardsson, A. Berning, D. L. Cooper, M. J. O. Deegan, A. J. Dobbyn, F. Eckert, E. Goll, C. Hampel, A. Hesselmann, G. Hetzer, T. Hrenar, G. Jansen, C. Köppl, Y. Liu, A. W. Lloyd, R. A. Mata, A. J. May, S. J. McNicholas, W. Meyer, M. E. Mura, A. Nicklass, D. P. O'Neill, P. Palmieri, D. Peng, K. Pflüger, R. Pitzer, M. Reiher, T. Shiozaki, H. Stoll, A. J. Stone, R. Tarroni, T. Thorsteinsson and M. Wang, MOLPRO, version 2015.1, a package of ab initio programs, 2015.
92. H. Lischka, D. Nachtigallová, A. J. A. Aquino, P. G. Szalay, F. Plasser, F. B. C. Machado and M. Barbatti, *Chemical Reviews*, 2018, **118**, 7293-7361.
93. J. V. Ortiz, in *Advances in Quantum Chemistry*, eds. J. Oddershede and E. J. Brändas, Academic Press, 2022, vol. 85, pp. 109-155.
94. M. D. Albaqami and A. M. Ellis, *Chem. Phys. Lett.*, 2018, **706**, 736-740.
95. P. Brockhaus, I. V. Hertel and C. P. Schulz, *J. Chem. Phys.*, 1999, **110**, 393-402.
96. J. Kozubal, T. R. Heck and R. B. Metz, *J. Phys. Chem. A*, 2019, **123**, 4929-4936.
97. J. I. Lee, D. C. Sperry and J. M. Farrar, *J. Chem. Phys.*, 2004, **121**, 8375-8384.
98. T. E. Salter and A. M. Ellis, *J. Phys. Chem. A*, 2007, **111**, 4922-4926.
99. L. Varriale, N. M. Tonge, N. Bhalla and A. M. Ellis, *J. Chem. Phys.*, 2010, **132**, 161101.
100. W. S. Hopkins, A. P. Woodham, N. M. Tonge, A. M. Ellis and S. R. Mackenzie, *J. Phys. Chem. Lett.*, 2011, **2**, 257-261.
101. T. Imamura, K. Ohashi, J. Sasaki, K. Inoue, K. Furukawa, K. Judai, N. Nishi and H. Sekiya, *Phys. Chem. Chem. Phys.*, 2010, **12**, 11647-11656.
102. K. Inoue, K. Ohashi, T. Iino, K. Judai, N. Nishi and H. Sekiya, *Phys. Chem. Chem. Phys.*, 2007, **9**, 4793-4802.
103. K. Inoue, K. Ohashi, T. Iino, J. Sasaki, K. Judai, N. Nishi and H. Sekiya, *Phys. Chem. Chem. Phys.*, 2008, **10**, 3052-3062.
104. N. Koga, K. Ohashi, K. Furukawa, T. Imamura, K. Judai, N. Nishi and H. Sekiya, *Chem. Phys. Lett.*, 2012, **539-540**, 1-6.
105. S. Li, B. R. Sohnlein, D.-S. Yang, J. Miyawaki and K.-I. Sugawara, *J. Chem. Phys.*, 2005, **122**, 214316.
106. J. Miyawaki and K.-i. Sugawara, *J. Chem. Phys.*, 2003, **119**, 6539-6545.
107. J. Miyawaki, D.-S. Yang and K.-i. Sugawara, *Chem. Phys. Lett.*, 2003, **372**, 627-631.
108. Y. Mune, K. Ohashi, T. Iino, Y. Inokuchi, K. Judai, N. Nishi and H. Sekiya, *Chem. Phys. Lett.*, 2006, **419**, 201-206.
109. M. Ogasawara, K. Shimizu, K. Yoshida, J. Kroh and H. Yoshida, *Chem. Phys. Lett.*, 1979, **64**, 43-45.
110. K. Ohashi, K. Inoue, T. Iino, J. Sasaki, K. Judai, N. Nishi and H. Sekiya, *J. Mol. Liq.*, 2009, **147**, 71-76.
111. T. Buttersack, P. E. Mason, R. S. McMullen, H. C. Schewe, T. Martinek, K. Brezina, M. Crhan, A. Gomez, D. Hein, G. Wartner, R. Seidel, H. Ali, S. Thürmer, O. Marsalek, B. Winter, S. E. Bradforth and P. Jungwirth, *Science*, 2020, **368**, 1086-1091.
112. S. Hartweg, A. H. C. West, B. L. Yoder and R. Signorell, *Angew. Chem. Int. Ed.*, 2016, **55**, 12347-12350.
113. M. T. J. H. Lodge, P. Cullen, N. H. Rees, N. Spencer, K. Maeda, J. R. Harmer, M. O. Jones and P. P. Edwards, *J. Phys. Chem. B*, 2013, **117**, 13322-13334.
114. M. Sprik, R. W. Impey and M. L. Klein, *Phys. Rev. Lett.*, 1986, **56**, 2326-2329.
115. H. Zhang and Z.-F. Liu, *J. Chem. Phys.*, 2012, **136**, 124314.
116. A. Kumar, J. A. Walker, D. M. Bartels and M. D. Sevilla, *J. Phys. Chem. A*, 2015, **119**, 9148-9159.
117. S. S. Xantheas, *J. Phys. Chem.*, 1996, **100**, 9703-9713.
118. Y. Tsuji, M. Hori and K. Yoshizawa, *Inorg. Chem.*, 2020, **59**, 1340-1354.
119. K. Maeda, M. T. J. Lodge, J. Harmer, J. H. Freed and P. P. Edwards, *J. Am. Chem. Soc.*, 2012, **134**, 9209-9218.
120. E. Zurek, X.-D. Wen and R. Hoffmann, *J. Am. Chem. Soc.*, 2011, **133**, 3535-3547.
121. A. G. Seel, P. J. Baker, S. P. Cottrell, C. A. Howard, N. T. Skipper and P. P. Edwards, *J. Phys. Chem. Lett.*, 2015, **6**, 3966-3970.
122. M. V. Ivanov, A. I. Krylov and S. Zilberg, *J. Phys. Chem. Lett.*, 2020, **11**, 2284-2290.
123. S. Nonose, T. Taguchi, F. Chen, S. Iwata and K. Fuke, *J. Phys. Chem. A*, 2002, **106**, 5242-5248.
124. J. V. Ortiz, I. Martín, A. M. Velasco and C. Lavín, *J. Chem. Phys.*, 2004, **120**, 7949-7954.
125. A. I. Boldyrev and J. Simons, *The Journal of Physical Chemistry*, 1992, **96**, 8840-8843.
126. B. A. Jackson and E. Miliordos, *J. Chem. Phys.*, 2022, **156**, 194302.
127. Z. Jordan, S. N. Khan, B. A. Jackson and E. Miliordos, *Electron. Struct.*, 2022, **4**, 015001.
128. E. A. Doud, A. Voevodin, T. J. Hochuli, A. M. Champsaur, C. Nuckolls and X. Roy, *Nat. Rev. Mater.*, 2020, **5**, 371-387.
129. J. Zhao, B. Li, K. Onda, M. Feng and H. Petek, *Chem. Rev.*, 2006, **106**, 4402-4427.
130. H. E. Zimmerman, *Acc. Chem. Res.*, 2012, **45**, 164-170.
131. A. J. Birch, *J. Chem. Soc.*, 1944, DOI: 10.1039/JR9440000430, 430-436.
132. E. Barwa, T. F. Pascher, M. Ončák, C. van der Linde and M. K. Beyer, *Angew. Chem. Int. Ed.*, 2020, **59**, 7467-7471.
133. T.-W. Lam, C. van der Linde, A. Akhgarnusch, Q. Hao, M. K. Beyer and C.-K. Siu, *ChemPlusChem*, 2013, **78**, 1040-1048.
134. C. van der Linde, A. Akhgarnusch, C.-K. Siu and M. K. Beyer, *J. Phys. Chem. A*, 2011, **115**, 10174-10180.
135. C. van der Linde, R. F. Höckendorf, O. P. Balaj and M. K. Beyer, *Chem. Eur. J.*, 2013, **19**, 3741-3750.
136. J. R. Christianson, D. Zhu, R. J. Hamers and J. R. Schmidt, *J. Phys. Chem. B*, 2014, **118**, 195-203.
137. J. P. Renault and S. Pommeret, *Radiat. Phys. Chem.*, 2022, **190**, 109810.
138. V. V. Rybkin, *J. Phys. Chem. B*, 2020, **124**, 10435-10441.
139. L. Zhang, D. Zhu, G. M. Nathanson and R. J. Hamers, *Angew. Chem. Int. Ed.*, 2014, **53**, 9746-9750.
140. D. Zhu, L. Zhang, R. E. Ruther and R. J. Hamers, *Nat. Mater.*, 2013, **12**, 836-841.
141. B. S. Bodnar and P. F. Vogt, *J. Org. Chem.*, 2009, **74**, 2598-2600.
142. J. R. Hwu, Y. S. Wein and Y.-J. Leu, *J. Org. Chem.*, 1996, **61**, 1493-1499.
143. R. Essmann, G. Kreiner, A. Niemann, D. Rechenbach, A.

- Schmieding, T. Sichla, U. Zachwieja and H. Jacobs, *Z. Anorg. Allg. Chem.*, 1996, **622**, 1161-1166.
144. D. W. Laorenza, A. Kairalapova, S. L. Bayliss, T. Goldzak, S. M. Greene, L. R. Weiss, P. Deb, P. J. Mintun, K. A. Collins, D. D. Awschalom, T. C. Berkelbach and D. E. Freedman, *J. Am. Chem. Soc.*, 2021, **143**, 21350-21363.
145. S. L. Bayliss, D. W. Laorenza, P. J. Mintun, B. D. Kovos, D. E. Freedman and D. D. Awschalom, *Science*, 2020, **370**, 1309-1312.
146. S. von Kugelgen, M. D. Krzyaniak, M. Gu, D. Puggioni, J. M. Rondinelli, M. R. Wasielewski and D. E. Freedman, *J. Am. Chem. Soc.*, 2021, **143**, 8069-8077.
147. M. R. Wasielewski, M. D. E. Forbes, N. L. Frank, K. Kowalski, G. D. Scholes, J. Yuen-Zhou, M. A. Baldo, D. E. Freedman, R. H. Goldsmith, T. Goodson, M. L. Kirk, J. K. McCusker, J. P. Ogilvie, D. A. Shultz, S. Stoll and K. B. Whaley, *Nat. Chem. Rev.*, 2020, **4**, 490-504.
148. J. Lehmann, A. Gaita-Ariño, E. Coronado and D. Loss, *J. Mater. Chem.*, 2009, **19**, 1672-1677.
149. I. Seidler, T. Struck, R. Xue, N. Focke, S. Trellenkamp, H. Bluhm and L. R. Schreiber, *Npj Quantum Inf.*, 2022, **8**, 100.
150. L. Gyongyosi and S. Imre, *Sci. Rep.*, 2021, **11**, 5172.
151. M. K. Wojnar, D. W. Laorenza, R. D. Schaller and D. E. Freedman, *J. Am. Chem. Soc.*, 2020, **142**, 14826-14830.
152. A. Albino, S. Benci, M. Atzori, L. Chelazzi, S. Ciattini, A. Taschin, P. Bartolini, A. Lunghi, R. Righini, R. Torre, F. Totti and R. Sessoli, *J. Phys. Chem. C*, 2021, **125**, 22100-22110.
153. A. Gaita-Ariño, F. Luis, S. Hill and E. Coronado, *Nat. Chem.*, 2019, **11**, 301-309.
154. M. J. Graham, J. M. Zadrozny, M. S. Fataftah and D. E. Freedman, *Chem. Mater.*, 2017, **29**, 1885-1897.
155. A. J. Campanella, Ö. Üngör and J. M. Zadrozny, *Comments Inorg. Chem.*, 2023, DOI: 10.1080/02603594.2023.2173588, 1-43.
156. A. K. Oanta, K. A. Collins, A. M. Evans, S. M. Pratik, L. A. Hall, M. J. Strauss, S. R. Marder, D. M. D'Alessandro, T. Rajh, D. E. Freedman, H. Li, J.-L. Brédas, L. Sun and W. R. Dichtel, *J. Am. Chem. Soc.*, 2023, **145**, 689-696.
157. G. Burkard, D. Loss and D. P. DiVincenzo, *Phys. Rev. B*, 1999, **59**, 2070-2078.
158. C.-J. Yu, S. von Kugelgen, D. W. Laorenza and D. E. Freedman, *ACS Cent. Sci.*, 2021, **7**, 712-723.
159. X. Wu, X. Liang, Y. Tian, F. Yang, C. Chen, Y.-C. Liu, M. K. Tey and L. You, *Chin. Phys. B*, 2021, **30**, 020305.
160. N. L. R. Spong, Y. Jiao, O. D. W. Hughes, K. J. Weatherill, I. Lesanovsky and C. S. Adams, *Phys. Rev. Lett.*, 2021, **127**, 063604.
161. C. S. Adams, J. D. Pritchard and J. P. Shaffer, *J. Phys. B: At. Mol. Opt.*, 2020, **53**, 012002.
162. M. Saffman, T. G. Walker and K. Mølmer, *Rev. Mod. Phys.*, 2010, **82**, 2313-2363.
163. M. Saffman, *J. Phys. B: At. Mol. Opt.*, 2016, **49**, 202001.
164. Z. Xiao, H. F. Drake, G. S. Day, J. E. Kuszynski, H. Lin, H. Xie, P. Cai, M. R. Ryder and H.-C. Zhou, *Cell Rep. Phys. Sci.*, 2022, **3**, 101074.
165. S. von Kugelgen and D. E. Freedman, *Science*, 2019, **366**, 1070-1071.
166. R. B. Somoano and J. C. Thompson, *Phys. Rev. A*, 1970, **1**, 376-383.
167. T. Goh, R. Pandharkar and L. Gagliardi, *J. Phys. Chem. A*, 2022, **126**, 6329-6335.